Detection of Brain Metabolites in Magnetic Resonance Spectroscopy

by

Trina Kok

B.Eng, Electrical and Computer Engineering
Duke University, 2005

Submitted to the Department of Electrical Engineering and Computer Science
in Partial Fulfillment of the Requirements for the Degree of

Master of Science in Electrical Engineering and Computer Science

at the

MASSACHUSETTS INTITUTE OF TECHNOLOGY

Feb 2009

Author_____
Department of Electrical Engineering and Computer Science
Dec 29, 2008

Certified by_____
Elfar Adalsteinsson
Associate Professor of Electrical Engineering and Computer Science
Associate Professor of Harvard-MIT Health Sciences & Technology
Thesis Supervisor

Accepted by_____
Terry P. Orlando
Professor of Electrical Engineering and Computer Science
Chairman, EECS Committee of Graduate Students

Detection of Brain Metabolites in Magnetic Resonance Spectroscopy

by

Trina Kok

Submitted to the
Department of Electrical Engineering and Computer Science

Dec 29, 2008

In Partial Fulfillment of the Requirements for the Degree of
Master of Science in Electrical Engineering and Computer Science

ABSTRACT

While magnetic resonance imaging (MRI) derives its signal from protons in water, additional and potentially important biochemical compounds are detectable in vivo within the proton spectrum. The detection and mapping of these much weaker signals is known as magnetic resonance spectroscopy or spectroscopic imaging. Among the complicating factors for this modality applied for human clinical imaging are limited chemical-shift dispersion and J-coupling that cause spectral overlap and complicated spectral shapes that limit detection and separation of several brain metabolites using MR spectroscopic imaging. Existing techniques for improved detection include so-called 2D spectroscopy, where additional encoding steps aid in the separation of compounds with overlapping chemical shift. This is achieved by collecting spectral data over a range of timing parameters and introducing an additional frequency axis, f1. Spectral editing techniques attempt to enhance metabolite signal detection along f1 in order to resolve specific metabolite signals. While these techniques have been shown to improve signal separation, they carry a penalty in scan time and more complicated reconstruction compared to conventional spectroscopy, and are often prohibitive when combined with spectroscopic imaging. The task of this thesis is to characterize and optimize existing 2D spectroscopy techniques for improved metabolite resolution with reduced number of timing steps through numerical simulation and experimental validation in phantoms.

Thesis Supervisor: Elfar Adalsteinsson
Title: Associate Professor of Electrical Engineering and Computer Science; Associate Professor of Harvard-MIT Health Sciences & Technology

Acknowledgements

The completion of most undertakings is seldom, if not never a solo effort. This thesis is possible through the efforts of many people.

In addition to directing me to interesting problems, I thank my advisor, Elfar for being always encouraging and patient with my work. His overflowing optimism and profound insight have been a great source of inspiration.

I would like to thank the members of the MRI group Borjan, Kawin, Div, Joonsung, Adam, Padraig and Audrey for their fruitful discussions and fantastic company. Borjan has helped me a lot in setting up and troubleshooting my sequences. Kawin, Joonsung and Div have provided me useful suggestions for improving my analysis and presentation.

My family is my pillar of support. I thank my dad and mom for always putting me first in their priorities for every decision they make, and for their encouraging and comforting weekly phone-calls. I also thank my brother who always calms my qualms with his sound advice.

My closest friends have brought me lots of cheer in the dismal winter days of Boston. I thank Naijia for his quiet fortitude and cheerful spirit. I thank Jinwei for standing by me all these years since high school despite my sparse contact. The Singaporean community at MIT has provided a home away from home and I really appreciate them for it.

I would like to acknowledge support from the National Science Scholarship of the Agency for Science, Technology and Research (A*STAR), Singapore.

Contents

List of Figures

List of Tables

1. Introduction

Nuclear Magnetic Resonance (NMR) was discovered independently by Felix Bloch [1] and Edward Purcell [2] in 1946. In the 1950's, NMR was used extensively in chemistry and physics for the evaluation of molecular structure and kinematics. In 1973, Paul Lauterbur demonstrated using linear gradient fields to spatially map molecules in a strong magnetic field. This opened up new applications for Magnetic Resonance Imaging (MRI), particularly in medical diagnostics for imaging soft tissue without the ionizing radiation effects of X-ray and Computer Tomography (CT) imaging.

In addition to anatomical imaging, magnetic resonance can also provide physiological and biochemical information via Magnetic Resonance Spectroscopic Imaging (MRSI, also known as chemical shift imaging (CSI)).

1.1. MRSI

MRSI is an imaging technique where one obtains a frequency spectrum of signals, e.g. brain metabolites in vivo, from an isolated volume of tissue. MRSI is based on the MR phenomenon of chemical shift, a subtle frequency shift in the signal that is dependent on the chemical environment of the particular compound. It is due to this frequency shift that there is a potential for physiological evaluation and material characterization of a volume of interest.

Chemical shift is defined as a small displacement of the resonance frequency due to shielding created by the orbital motion of the surrounding electrons in response to the main B_0 field. By placing a sample of material in a uniform magnet, exciting it, recording the signal from its Free Induction Decay (FID), and then Fourier transforming the FID, the resultant MR spectrum shows resonances at different frequencies corresponding to different chemical shifts

[3]. The amount of displacement and the amplitude of the peaks in the spectrum depend on the molecular structure of the compound of interest.

In the presence of the main magnetic field Bo, the effective field experienced by the nucleus is

$$B_{eff} = B_0 - B_0\sigma = B_0(1-\sigma) \tag{1.1}$$

where σ represents a shielding constant dependent on the chemical environment. From the Larmor relationship, we can write the above equation as

$$\omega_{eff} = \omega_0 - \omega_0\sigma = \omega_0(1-\sigma) \tag{1.2}$$

where $\omega_0\sigma$ is the displacement of the resonant frequency. Thus the change in frequency is proportional to the magnetic field B_0. By expressing this displacement in resonant frequency in units of "parts per million" (ppm) with respect to a reference frequencyω_R, the displacement in frequency can be compared across scans with different main magnetic field B_0 strengths. If the resonant frequency of the sample is ω_s, then the chemical shift δ in ppm is

$$\delta = \frac{\omega_s-\omega_R}{\omega_R} \times 10^6 = \frac{\sigma_s-\sigma_R}{1-\sigma_R} \times 10^6 \approx (\sigma_s - \sigma_R) \times 10^6 \qquad \text{because } \sigma_R \ll 1 \tag{1.3}$$

The frequency axis in MRSI, for historical reasons, is such that the frequency decreases from left to right. Figure 1 shows an example of such a spectrum which is the ^1H spectrum of acetic acid (CH_3COOH). The three protons of the CH_3 experience a different chemical shift than the proton in the COOH group. The valency of the oxygen in the COOH group leads to an attraction of the electron away from the proton, so that there is less shielding for the proton in the COOH group compared to the protons in the CH_3 group and the resonant frequency for COOH deviates more from the reference frequency.

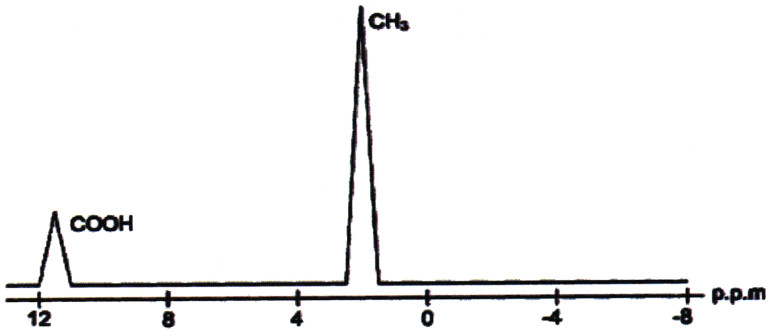

Figure 1.^{1}H NMR spectrum of acetic acid (CH_3COOH)

1.2. J-coupling

In addition to chemical shifts caused by the shielding of electrons, subtle chemical shifts also result from J-coupling effects within molecules. Nuclei which are close to one another in chemical shift exert an influence on each other's magnetic field and this influence is known as J-coupling. Consider a molecule containing two different spin-½ nuclei, A and M, where their nuclei could be either spin-up (+½) or spin-down (-½). Without any J-coupling, we would expect one line of resonance in the frequency spectrum obtained from spectroscopic imaging of either

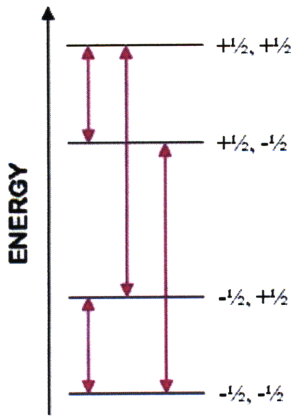

Figure 2. Energy transitions for two spins that are weakly coupled

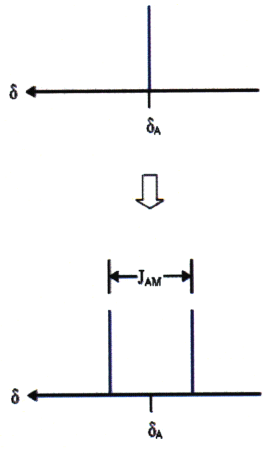

Figure 3. Line splitting due to weak coupling results in two lines of resonance separated by the coupling constant J_{AM}

change is allowed in one transition, so the four possible spin configurations of A and M results in four different transitions in Figure 2- two for nucleus A and two for nucleus M [4]. Thus, the frequency spectrum obtained from MRSI of nucleus M (or A) exhibits two lines of resonance with reduced amplitudes instead of a single line of resonance in Figure 3. This effect is known as line-splitting.

1.3. 2D MRS

By introducing an additional time variable, a 2D frequency spectrum of metabolites could be obtained. The additional time variable encompasses additional information on nuclear interactions including J-coupling information. The simplest 2D MRS sequence comprises two 90° pulses with two time variables t_1 and t_2. Figure 5 is an example of such a sequence. Magnetization is allowed to precess freely in t_1 before FID detection during t_2. Repeating the experiment for a range of t_1 values leads to a two dimensional set of NMR data which can be Fourier transformed in both dimensions to obtain a 2D frequency spectrum in ω_1 and ω_2. The 2D frequency spectrum reveals coupling information between different metabolites.

1.4. Problem statement

The spectrum in Figure 4 is an example of in vivo signal from human brain, with amount of signal contributed from the water and the lipid groups in the scanned volume significantly suppressed by means of applying RF pulse that was spectrally selective. This is crucial in MRSI, since the metabolite signals of interest are of very small concentration compared to the water and fat signals (1-10 mM for observable brain metabolites in vivo vs. ~50M for water). Therefore, spectroscopy scans have intrinsically low SNR compared to conventional MRI of water [5].

However, low SNR is not the only challenge in MRSI. Line splitting caused by J-coupling between different nuclei of the same compound further reduces the SNR of the frequency spectrum of the metabolites. Complicated J-coupling results in multiplets for a single metabolite and these multiplets often overlap with the spectra of other metabolites, thus making metabolite quantification and detection difficult.

In addition, inherent B_0 and B_1 inhomogeneities depend on several factors, including main field strength, RF coil design, and subject-induced magnetic susceptibility variations, and further complicate low-SNR metabolite estimates. Other types of signal contaminations, such as patient movement, contribute to the challenge of obtaining spectroscopic images of high quality.

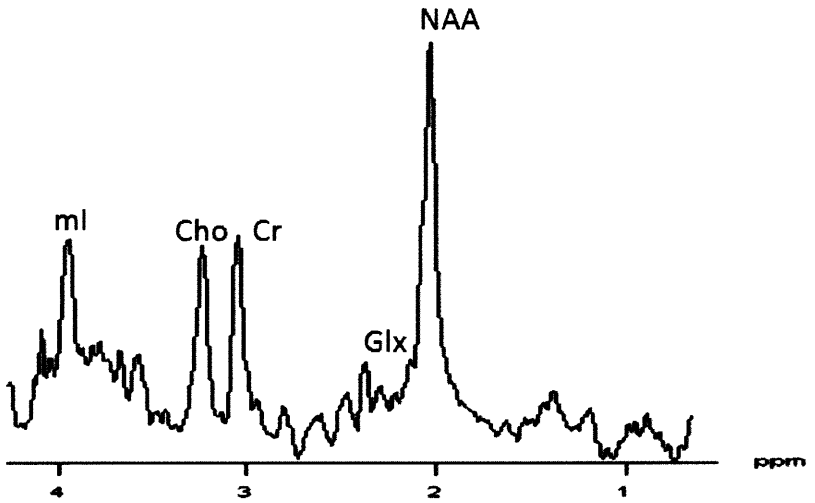

Figure 4. A typical human brain metabolite spectrum from a 1D spin-echo acquisition at 3T with TE/TR = 35ms/2s for a voxel size of 8cc at 1000Hz bandwidth, 20 averages and 1024 ADC points.

1.5. Contributions

Several factors complicate quantification of brain metabolites, including inhomogeneities in the B_0 and B_1 fields. To enable comparison across subjects under different scanning conditions, expressing the metabolite signals as ratios to the sum of the metabolite signal from Cr and PCr (Cr') is a common technique, which while providing robustness to factors such as partial voluming and B_1 inhomogeneities, relies on inherent assumptions about the stability of a

reference signal (often Cr). Work presented in this thesis extends compartmental analysis of absolute metabolite measures to ratio measure, with applications to human imaging at 7T in adrenoleukdoystrophy (ALD) [6][7].

A second contribution of this thesis concerns 2D MRS. These methods require stepping through a range of times in order to obtain a 2D metabolite spectrum, which can yield improved spectral information for coupled or overlapping spin systems compared to conventional 1D chemical shift spectroscopy. The number of time steps depends on the methods used and typically ranges from 16 to 128 steps. By observing the different J-modulation effects on metabolites of interests at different time steps, it is possible to obtain some combination of metabolite spectra that will result in better resolution of metabolites. This work explores the potential combination of metabolite spectra that may contribute to a better detection of metabolites.

1.6. Organization

The remainder of this thesis is as follows. Chapter 2 contains a more detailed description of 2D MRS and spectral editing, and the predominant methods for resolving the metabolites Glutamate (Glu) and Glutamine (Gln). Chapter 3 contains the extension of compartmental analysis of MRSI absolute metabolite measures to ratio measures. Chapter 4 contains the analysis from simulated spectra of CT-PRESS, 2DJ-PRESS, TE-averaging PRESS and concatenated spectra. Chapter 5 contains the analysis of spectra of CT-PRESS, 2D-JPRESS, TE-averaging PRESS and concatenated spectra obtained from a 3T MRI scanner (Siemens, Erlangen, Germany). Discussion of the results and future work is presented in Chapter 6.

Bibliographical Note

The problem formulation and the results of Chapter 3 have been presented at the following meeting:

- Kok T, Ratai E-M, Eichler F, Adalsteinsson E, "Analysis of 1H Metabolite Ratios Using Image Segmentation at 7T in adult patients with X-linked Adrenoleukodystrophy", Toronto, Canada, ISMRM Proc., #1596
- Ratai E, Kok T, Wiggins C, Wiggins G, Grant E, Gagoski B, O'Neill G, Adalsteinsson E, Eichler F, "Seven-Tesla proton magnetic resonance spectroscopic imaging in adult X-linked adrenoleukodystrophy," Arch Neurol. 2008 Nov;65(11):1488-94.

2. 2D MRS

2.1. Motivation

2D MR spectroscopy introduces a second frequency axis to chemical shift spectroscopy. By notational convention, ω_2 (or f_2) is used to resolve chemical shift, while ω_1 (f_1) encodes additional physical characteristics of the underlying spins, often J-coupling or a combination of J-coupling and chemical shift. The time variables corresponding to ω_1 and ω_2, are t_1 and t_2. The precise meaning of the additional frequency axis ω_1 depends on the kind of experiment performed. There exist a number of different 2D MRS experiments [8], and this thesis will focus on those experiments that attempt to resolve glutamate (Glu) and glutamine (Gln) for human brain spectroscopy at 3T. Glutamate is the most abundant amino acid found in the brain at approximately 12 mM/kg [9], and acts as an excitatory neurotransmitter. Glu has four protons in two methylene groups at 2.0375ppm, 2.1200ppm, 2.3378pm and 2.3520ppm, and one proton in a methine group at 3.7433ppm that are strongly coupled with one another, giving a complex spectrum at 3T with low-intensity multiplets. The coupling constants and chemical shifts are summarized in Table 1. The Glu spectrum overlaps with resonances of Gln, γ-Aminobutyric acid (GABA) and N-Acetyl aspartate (NAA), making detection and quantification in vivo difficult. Gln is a storage form of Glu and is present in the range of 2-4 mM/kg [9]. A large increase of Gln occurs when the Glu/Gln cycle is altered with disease [10][11]. Gln has four protons in two methylene groups at 2.1090ppm, 2.1290ppm, 2.4320ppm and 2.4540ppm and another proton in a methine group at 3.7530ppm that are strongly coupled at 3T. The coupling constants and chemical shifts of Glu and Gln as reported from Ref. [9] are summarized in Table 1. Separation of Gln and Glu is very difficult at low field, and this thesis explores methods to resolve the two metabolites.

Metabolite	Group		Chemical shift (ppm)	Connectivity	Coupling Constant J (Hz)
Glutamate	1	CH	3.7433	1-2	7.331
	2	CH_2	2.0375	1-2'	4.651
	2'		2.1200	2-2'	-14.849
	3	CH_2	2.3378	2-3'	8.406
	3'		2.3520	2'-3'	6.875
				2-3	6.413
				2'-3	8.478
				3-3'	-15.915
Glutamine	1	CH	3.7530	1-2	5.847
	2	CH_2	2.1290	1-2'	6.500
	2'		2.1090	2-2'	-14.504
	3	CH_2	2.4320	2-3	9.165
	3'		2.4520	2-3'	6.347
				2'-3	6.324
				2'-3'	9.209
				3-3'	-15.371

Table 1. Chemical shifts and coupling constants of protons in Glu and Gln as reported in [9] which are used in simulation studies in chapter 4

2.2. 2DJ-PRESS

In 2DJ-PRESS [12], data is acquired as a function of t_1 = TE and t_2 = time and Fourier transformed in both t_1 and t_2 domains. The timing sequence is shown in Figure 5. Because J-coupling manifests itself in both f_1 and f_2, the spectrum for coupled spins is tilted along the 45°-axis in the (f1, f2) plane. In post-processing, the 2D spectrum is tilted by 45° along the diagonal to obtain the J-coupling information in f_1 and chemical shift information in f_2. Since the signal is distributed amongst the coupled peaks, the SNR for each peak in the 2D frequency spectrum is decreased compared to equal concentration of a singlet.

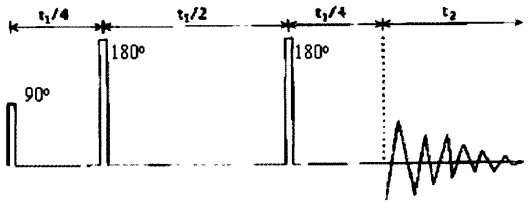

Figure 5. Pulse sequence of 2DJ-PRESS [12]

2.3. CT-PRESS

In CT-PRESS [13], a refocusing 180° pulse of the sequence is shifted within a constant time interval between RF excitation and signal acquisition. The scheme is shown in Figure 6. Cross-peaks in the 2D Fourier representation indicating J-coupling are eliminated because magnetization is not transferred to the cross-peaks. All magnetization is instead transferred to the diagonal spectrum which contains signals of all uncoupled spins and diagonal peaks of coupled spins. Thus, the SNR from the diagonal spectrum is increased compared to 2DJ-PRESS. SNR of coupled resonances can be further increased by optimizing the timing parameter t_c for the size and number of spin couplings. However, CT-PRESS requires a considerably larger number of t_1 steps compared to 2DJ-PRESS. About 128 t_1 steps are required for a ^1H chemical shift range of 5-10ppm with sufficient spectral resolution. It is possible to reduce the number of TE steps by noting that only signals near the diagonal will appear in the 2D CT-PRESS spectrum. Nyquist sampling theorem can be violated and this has been demonstrated by Mayer et al [14].

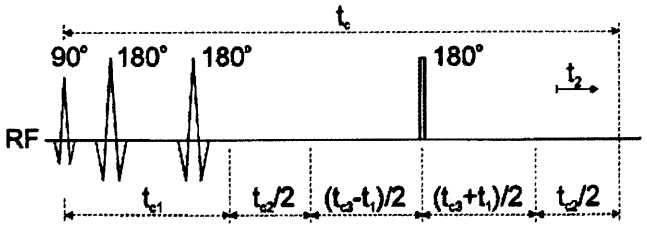

Figure 6. Pulse sequence of CT-PRESS [13]

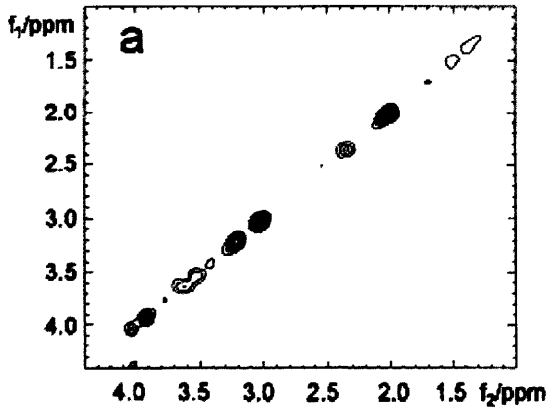

Figure 7. An example 2D spectrum of a healthy rat brain. Cross-peaks are eliminated as energy is only deposited on the diagonal of the spectrum. [13]

2.4. *TE-averaging PRESS*

TE-averaging with a PRESS sequence [15] has been studied for resolving glutamate signal (Glu) from brain metabolites at 3T. Similar to 2DJ-PRESS, metabolite data is acquired for a range of TE but Fourier transformed only in the t_1 domain. An average of the data from different TE's is taken and this average represents the f_1=0 component of a 2D J-PRESS spectrum. Glu is reasonably resolved at 16 and 32 TE steps but the closely correlated metabolite glutamine (Gln) is difficult to obtained directly.

2.5. *Spectral Editing*

Spectral editing is a method of suppressing or enhancing metabolite signals by using its spin-spin coupling properties. Due to the effects of J-modulation, different timing parameters result in different metabolite spectra that can be manipulated to resolve the metabolite of interest. Spectral editing has been exploited in [16] to resolve Glu from an in vivo spectrum at 1.5T by the subtraction of metabolite spectra from TE = 12ms and TE = 60ms. However, resolution of Gln is difficult because of the strong correlation between Glu and Gln.

3. Compartmental analysis with 1D MRSI

In 1D spectroscopy, absolute metabolite concentrations are estimated from experimental metabolite data via models such as LCmodel [17], which attempts to account for complexities arising from macromolecular baseline, J-coupling, multiplets and metabolite signal overlaps. The combination of low-SNR spectroscopy with segmented structural data has been used to provide brain metabolite estimates in separate tissue compartments [18]. Factors such as partial voluming, coil loading and inhomogeneities in the B_0 and B_1 fields under different scanning conditions are challenges to using absolute metabolite estimates for quantification purposes. To correct for comparison across subjects under these different scanning conditions, expressing the metabolite signals as ratios to the sum of the metabolite signal from Cr and PCr (Cr') is a common technique. The work in this chapter extends compartmental analysis of absolute metabolite measures to ratio measure. The detection of metabolites such as NAA provides an indication of neuronal function and could help characterize axonal integrity in X-linked adrenoleukodystrophy (X-ALD).

3.1. Model for Metabolite Ratio Analysis Combined with Segmented Structural Imaging

The model for the gray and white mater contribution to the signal observed for metabolite M is based on the following model from Ref. [19].

$$y_i = g_i \cdot M_g + w_i \cdot M_w + n_i \tag{3.1}$$

where y_i is the measured metabolite signal, g_i and w_i are the structural representations of the gray and white matter, M_g and M_w are the gray and white matter contributions to the signal for metabolite M, and n_i is the additive Gaussian noise. By expressing M_w/M_g as $r_{gw,}$, a nonlinear

two-dimensional search for M_g and M_w is avoided so that we need only estimate one nonlinear parameter r_{gw} and one nonlinear parameter M_w.

$$y_i = M_w \left(g_i \cdot r_{gw} + w_i \right) + n_i \tag{3.2}$$

Using the method of variable projection [20], the least square solution is found first by expressing the estimate $\tilde{M}_w$ assuming r_{gw} is known, as

$$\tilde{M}_w = \frac{\sum_{i=1}^{N} f_i \cdot y_i}{\sum_{i=1}^{N} f_i^2} \tag{3.3}$$

where

$$f_i = g_i \cdot r_{gw} + w_i \tag{3.4}$$

and N is the total number of spectroscopic voxels used in the analysis.

The estimated gray to white ratio $\tilde{r}_{gw}$, is found by evaluating Eq.5 after substituting Eq. 3 into Eq. 2.

$$\min_{r_{gw}} \sum_{i=1}^{N} \left| y_i - \tilde{M}_w f_i \right| \tag{3.5}$$

Upon finding the optimum value for $\tilde{r}_{gw}$, $\tilde{M}_w$ was found via Eq. 3, and $\tilde{M}_g$ determined via Eq. 6.

$$\tilde{M}_g = \tilde{M}_w \cdot r_{gw} \tag{3.6}$$

We would like to obtain a model for the signal observed for the metabolite *M* as a ratio to the signal observed for Cr'. Using Eq. 1, the ratio r_i of the signal observed for metabolite *M* to the signal observed for Cr', then becomes

$$r_i = \frac{y_{i_M}}{y_{i_{Cr'}}} = \frac{g_i \cdot M_g + w_i \cdot M_w + n_{i_M}}{g_i \cdot Cr'_g + w_i \cdot Cr'_w + n_{i_{Cr'}}} \tag{3.7}$$

$$r_i = \frac{g_i \cdot M_g}{g_i \cdot Cr'_g + w_i \cdot Cr'_w + n_{i_{Cr'}}} + \frac{w_i \cdot M_w}{g_i \cdot Cr'_g + w_i \cdot Cr'_w + n_{i_{Cr'}}} + \frac{n_{i_M}}{g_i \cdot Cr'_g + w_i \cdot Cr'_w + n_{i_{Cr'}}} \tag{3.8}$$

$$r_i = \frac{g_i}{g_i + w_i \cdot \frac{Cr'_w}{Cr'_g} + \frac{n_{i_{Cr'}}}{Cr'_g}} \left(\frac{M_g}{Cr'_g} \right) + \frac{w_i}{w_i + g_i \cdot \frac{Cr'_g}{Cr'_w} + \frac{n_{i_{Cr'}}}{Cr'_w}} \left(\frac{M_w}{Cr'_w} \right) + \frac{n_{i_M}}{g_i \cdot Cr'_g + w_i \cdot Cr'_w + n_{i_{Cr'}}} \tag{3.9}$$

The model for the metabolite ratio observed in a particular voxel r_i for the metabolite M is

$$r_i = g''_i \cdot \left(\frac{M_g}{Cr'_g} \right) + w''_i \cdot \left(\frac{M_w}{Cr'_w} \right) \tag{3.10}$$

$$g''_i = \frac{g_i}{g_i + w_i \cdot \frac{Cr'_w}{Cr'_g}} \qquad w''_i = \frac{w_i}{w_i + g_i \cdot \frac{Cr'_g}{Cr'_w}} \tag{3.11}$$

We aim to determine the optimal values of the global quantities M_g /Cr'_g and M_w /Cr'_w for each subject, which are the gray and white matter contributions to the metabolite M expressed as ratios to the gray and white matter contributions to the metabolite Cr'. M_g /Cr'_g and M_w /Cr'_w indicate the amount of metabolite signal ratio r_i for particular g_i'' and w_i'' in a certain voxel. Cr'_g and Cr'_w were obtained by estimating $r_{gw} = Cr'_g / Cr'_w$ using the absolute metabolite data of Cr' from each voxel of the subject. This estimate of r_{gw} was then used to determine g_i'' and w_i''. With g_i'' and w_i'' expressed as shown, the procedure for finding the optimal values of M_g /Cr'_g and M_w /Cr'_w is equivalent to the procedure for finding the optimal values of M_g and M_w of Eq. 1 where g_i is substituted by g_i'' and w_i *is* substituted by w_i''.

3.2. Method

All imaging was done on a 7.0T MRI scanner (Siemens AG, Erlangen, Germany). The spectroscopic VOI for the 2D ^{1}H MRSI was selectively excited using PRESS (TE = 35ms, TR = 2s) with CHESS water suppression and six spatial outer volume suppression pulses for fat suppression. A spectroscopic voxel size of 2.3cm^3 resulted from partition the FOV of 20cm with 16 x 16 phase encoding steps. The spectra bandwidth was 4000Hz and the water suppression bandwidth was 120Hz. The structural image at a resolution of 0.56 x 0.56 x 1 mm^3 = 0.31 mm^3 were acquired with an axial MPRAGE sequence with timing parameters TE/TR/TI = 3.6/2500/1100 ms.

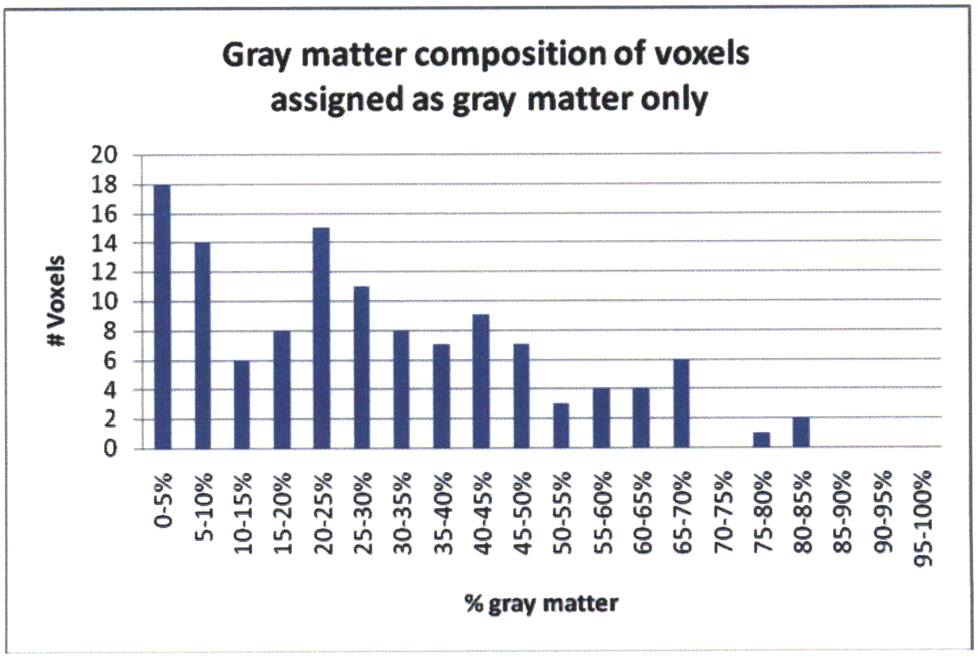

Figure 8. Gray matter composition determined from segmented structural data assuming rectangular solid voxels for spectroscopic voxels assigned as containing gray matter only.

We demonstrate the use of the model for the metabolite ratio for data obtained from twelve ALD patients and nine healthy subjects. The gray and white matter composition of each of the subject's structural image was determined by a combination of automated segmentation using Freesurfer [21][22] and manual segmentation, and registered to the spectroscopic data.

We assumed an idealized rectangular function for the point spread function of the structural acquisition and for the spectroscopy. In a previous analysis [7][23], only spectroscopic voxels manually assigned as containing 100% white matter (predominantly white) or 100% gray matter (predominantly gray) were used. Figure 8 and Figure 9 illustrate the gray and white matter composition as determined from segmentation of the spectroscopic voxels that were previously manually assigned as containing 100% white matter or 100% gray matter. For the voxels assigned as containing 100% gray matter, the gray matter content is significantly overestimated.

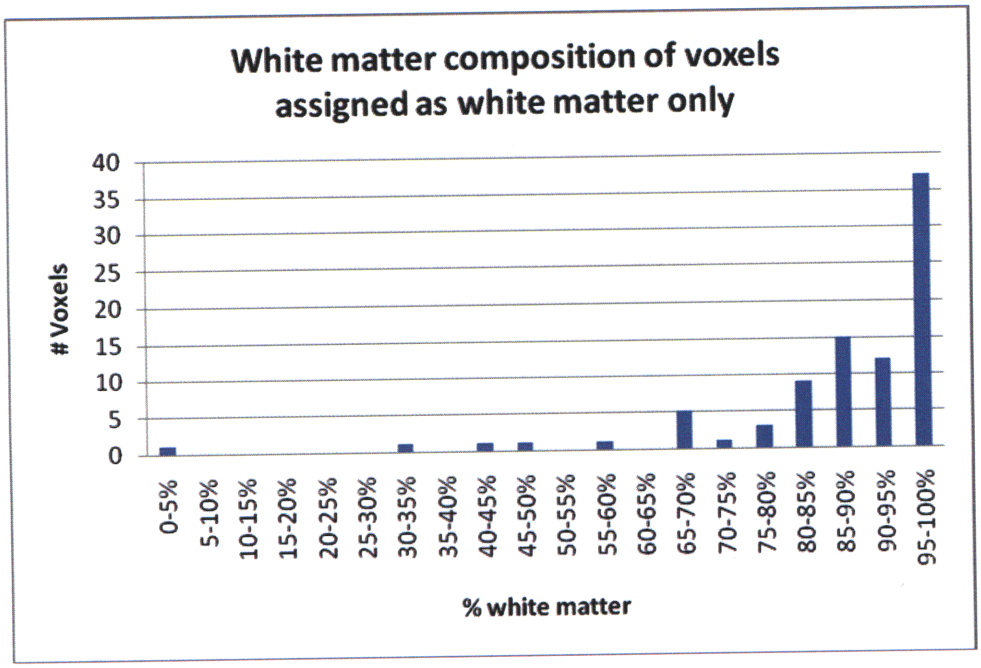

Figure 9. White matter composition determined from segmented structural data assuming rectangular solid voxels for spectroscopic voxels assigned as containing white matter only.

For the voxels assigned as containing 100% white matter, the assignment approximates the content better. This is due to the fact that the anatomy of the selected VOI is such that gray-matter voxels of full volume are less common than those of white matter. To better reflect the content of gray and white matter and their corresponding changes in metabolite concentrations, we incorporated segmented structural data for the same set of spectroscopic voxels into the analysis of ratios for the following four metabolites, NAA' (N-Acetyl-Aspartyl-Glutamate(NAAG)

+ NAA), myo-Insitol (Ins), Cho' (Glycero-phosphoryl-choline (GPC) + Phosphoryl-choline (PC)) and Glx (Glu and Gln). This corrected metabolic segmentation has relevance to the monitoring of demyelination and axonal degeneration in X-ALD.

3.3. Results and Discussion

Figure 10, Figure 11, Figure 12 and Figure 13 are examples of the analysis applied to NAA', Ins, Cho' and Glx of ALD patients. The z-axis shows values of the metabolic ratio r_i and the x and y-axis shows values of g_i'' and w_i'' respectively. The red crosses ('**x**') in the figure are obtained by manually assigning spectroscopic voxels as either 100% gray or 100% white. The averages of r_i for both the 100% gray-matter and 100% white matter voxels are shown in purple ('•'). Based on the segmentation, most of these spectroscopic voxels are mixed-volume and their composition is represented by the black triangles in the figure ('▼'). Using these mixed-volume data and applying our model, we obtained an estimate M_g /Cr'_g and M_w /Cr'_w for each ALD patient and averaged these values across the patients. With the averaged M_g /Cr'_g and M_w /Cr'_w, the metabolite ratio r_i is expressed as a function of g_i'' and w_i'' in Eq. (3.1) and represented by the blue line ('—') in Figure 10. The green lines ('—') of Figure 10 indicate one standard deviation from the averaged values.

The same procedure in obtaining Figure 10, Figure 11, Figure 12 and Figure 13 is repeated for obtaining Figure 14, Figure 15, Figure 16, and Figure 17 for the control subjects. The M_g /Cr'_g and M_w /Cr'_w obtained from this analysis offers a comparison metric for changes in metabolite levels between ALD patients and healthy subjects and we demonstrate its use as such a metric in Figure 18 where an ANOVA test was done and a significant decrease of NAA' in both the gray and white matter of ALD patients was found.

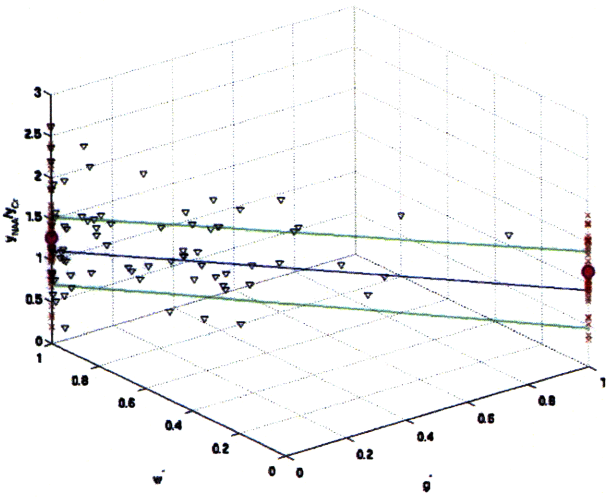

Figure 10. Analysis of NAA' for ALD patients

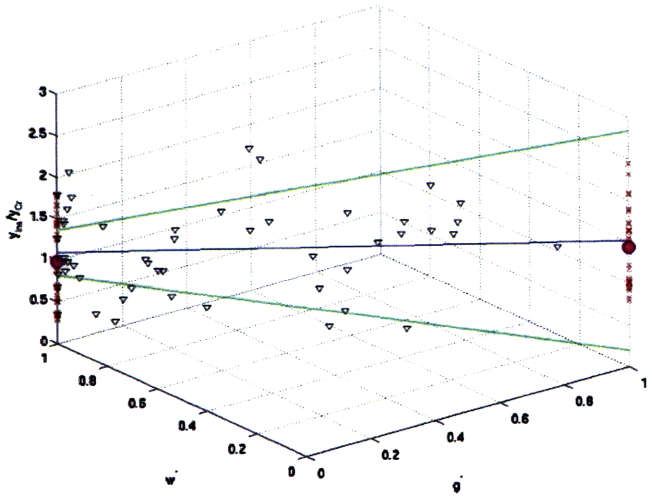

Figure 11. Analysis of Ins for ALD patients

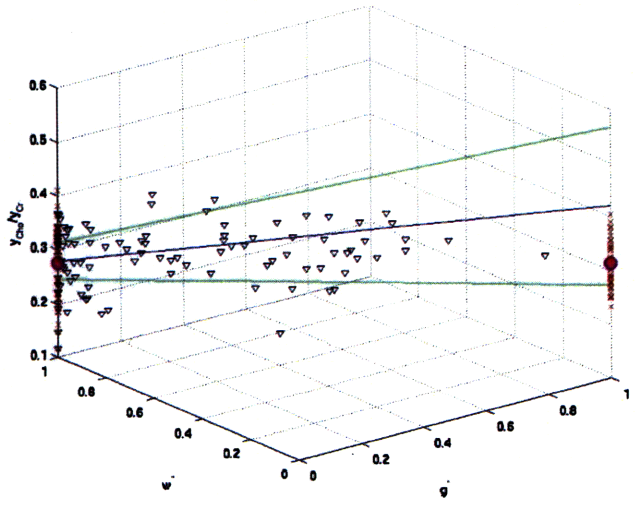

Figure 12. Analysis of Cho' for ALD patients

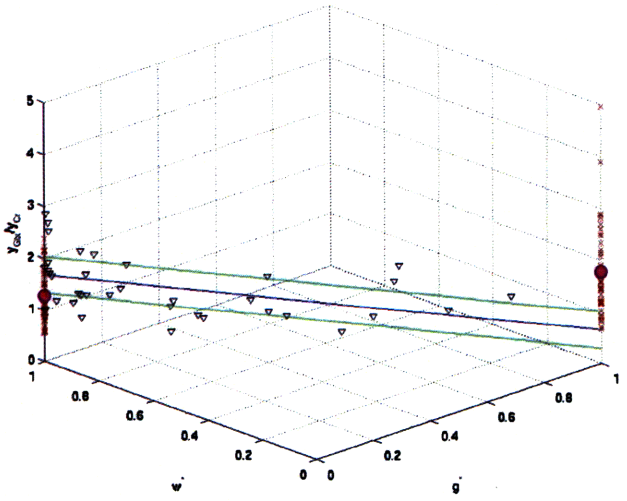

Figure 13. Analysis of Glx for ALD patients

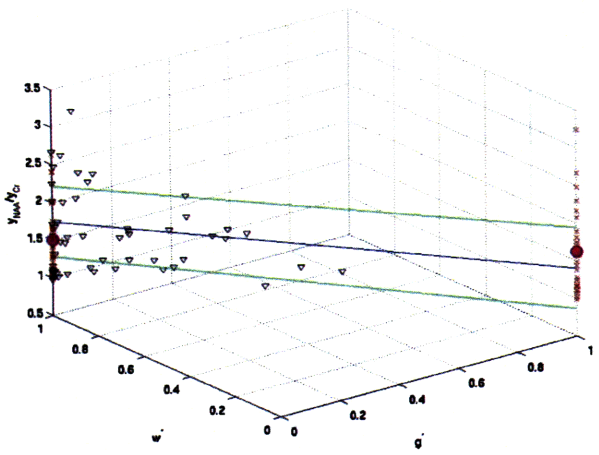

Figure 14. Analysis of NAA' for control patients

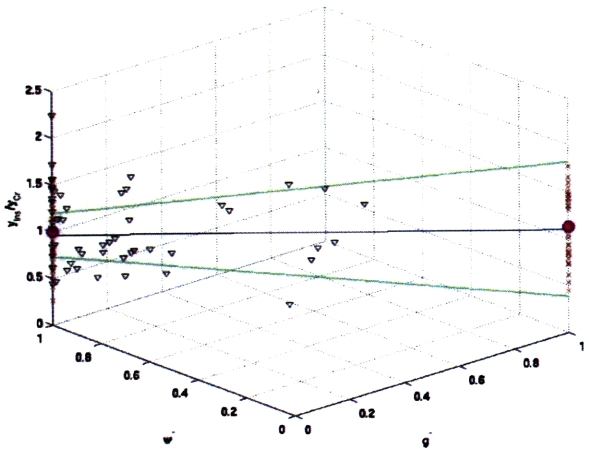

Figure 15. Analysis of Ins for control patients

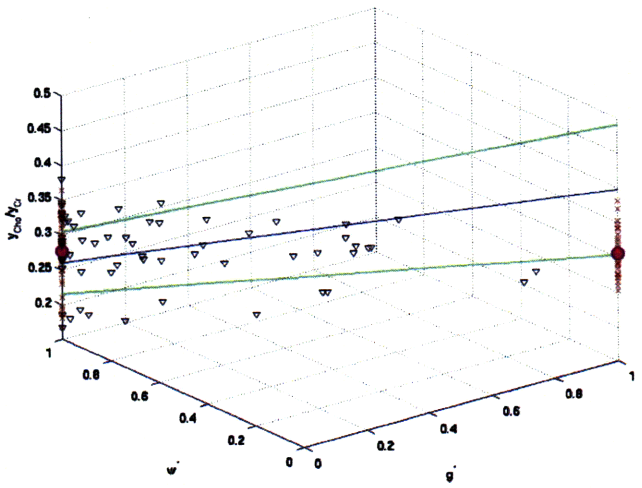

Figure 16. Analysis of Cho' for ALD patients

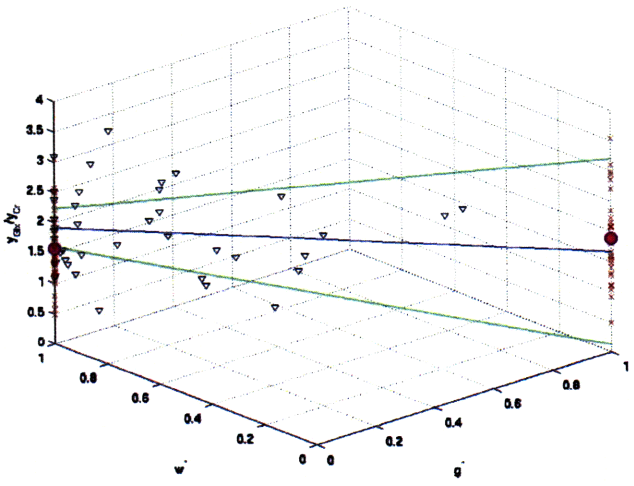

Figure 17. Analysis of Glx for ALD patients

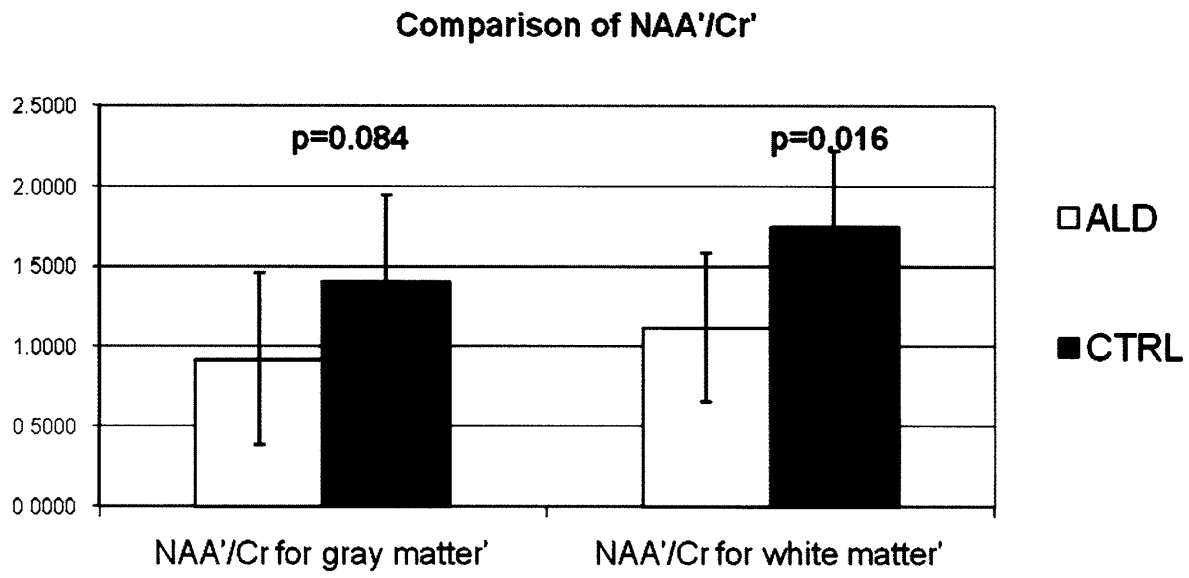

Figure 18 Comparison between ALD and control subjects for the global values of NAA'/Cr shows a significant decrease in both gray (p = 0.084) and white matter (p=0.016) in ALD patients. P-values are obtained from an ANOVA test.

4. Numerical simulations of idealized excitation for 2DJ-PRESS and CT-PRESS

2D MRS methods of 2DJ-PRESS and CT-PRESS were simulated with a software package SPINEVOLUTION [24] according to timing parameters given in Ref. [15] and Ref. [13]. The performance of these 2D MRS methods were compared with the 1D spin-echo method at TE=35ms, in terms of the accuracy of the estimation of the concentrations of the following metabolites creatine (Cr), N-acetylaspartate (NAA), glutamate (Glu) and glutamine (Gln). Metabolite NAA is included because part of its spectra centered at 2.008 ppm overlaps with the Glu multiplet centered at 2.05ppm and may potentially complicate the estimation of Glu and Gln. Metabolite Cr is added in the study because it consists only of 2 singlets and serves as an appropriate control metabolite across the 1D and 2D MRSI methods. Simulation input files for the simulated spectra of Glu of the 2DJ-PRESS, CT-PRESS and 1D spin-echo acquisitions are included in the appendix.

4.1. 2D-MRS and 1D methods

In TE-averaging PRESS, the f1=0 component of the 2D spectrum from a 2DJ-PRESS experiment forms a 1D spectrum from which Glu is resolved [15]. In addition to evaluating the performance of this 1D TE-averaged spectrum in estimating individual metabolite concentrations, the performance of a spectrum obtained from the concatenation of individual FID's obtained from each TE value of the 2DJ-PRESS experiment was evaluated. In the rest of this thesis, this concatenated spectrum is referred to as 2DJ-PRESS-concatenated. The performance of the 1D spectra obtained from individual TE steps of the 2DJ-PRESS experiment was also analyzed and compared with the TE-averaged spectrum and the spectrum obtained from the concatenated FID's.

In CT-PRESS, the projection of the 2D spectrum onto the f1 axis results in a 1D spectrum from which metabolites are reported reliably resolved [13]. The performance of this projected 1D-spectrum was compared with the performance of the spectrum obtained from the concatenation of individual FID's at each t_1 step of the CT-PRESS experiment. In the rest of this thesis, this spectrum is referred to as CT-PRESS-concatenated. In addition, the performance of the 1D spectra from each individual t_1 step were evaluated and compared with the spectra obtained from the concatenated FID's and the projected spectrum.

4.2. Simulation with SPINEVOLUTION

The pulse sequences for the 2DJ-PRESS, CT-PRESS and 1D spin-echo experiments were implemented in script files which were in turn inputted to the SPINEVOLUTION program. The simulation implemented as single voxel experiments and was executed with very short rectangular 90° and 180° RF pulses of length 0.5us, assuming a 3T main magnetic field.

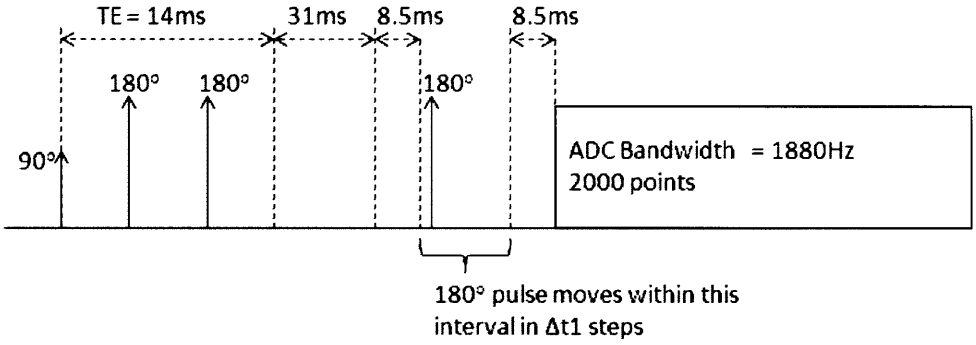

Figure 19. Timing parameters for the CT-PRESS experiment. PRESS was implemented with TE = 14ms. The location of the last 180o pulse is varied within a fixed interval and the ADC readout starts at a fixed time relative to the 90° excitation pulse.

Cross-referencing Figure 19, the press sequence was implemented with TE = 14ms, and 128 t_1 steps were taken with Δt_1 = 0.133ms. The spectra bandwidth in both f_1 and f_2 were 1880Hz. The 2DJ-PRESS experiment was implemented with TE ranging from 35ms to 185ms in

increments of 10ms and at a spectra bandwidth of 5000Hz with 2000 ADC points. The TE-averaged spectrum and concatenated spectrum are obtained from this 16-step 2DJ-PRESS experiment. In order to study the effects of shorter TE times, a 38-step 2DJ-PRESS experiment was simulated with TE ranging from 5ms to 190ms in increment of 5ms and a spectra bandwidth of 5000Hz with 2K ADC points.

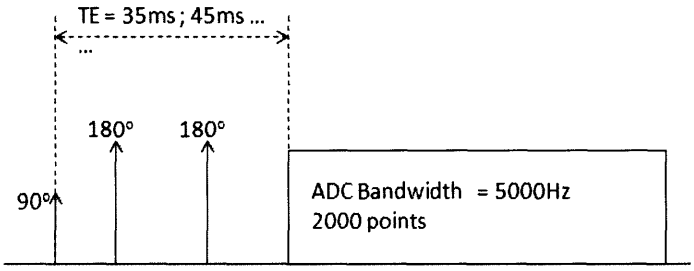

Figure 20. Timing parameters for the 16-step 2DJ-PRESS experiment. PRESS was implemented with varying 35ms< TE < 185ms in 10ms increments. ADC readout is shifted along with the varying TE

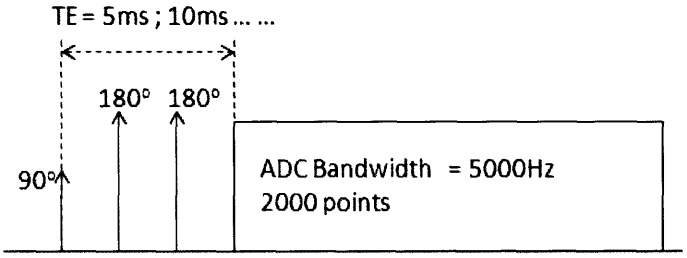

Figure 21. Timing parameters for the 38-step 2DJ-PRESS experiment. PRESS was implemented with varying 5ms< TE < 190ms in 10ms increments.

A separate input file was written for each of Cr, NAA, Glu and Gln incorporating their respective chemical shift and J-coupling constants reported in [9]. The relaxation times of Cr-CH_3 and Cr-CH_2 were inputted as T1 = 1.29s and T2 = 165ms, and T1 = 890ms and T2 = 126.5ms respectively. The relaxation times of NAA were inputted as T1 = 1.365s and T2 = 265ms. These relaxation times were obtained by averaging the reported relaxation times for

each metabolite at 3.0T across different brain regions [25]. For Glu, relaxation times were inputted as T1 = 1.2s [26] and T2 = 200ms [27]. The relaxation times for Gln were simulated to be the same as Glu due to the lack of published studies on T1 and T2 times of Gln at 3.0T.

4.3. Estimation using simulated spectra

Using the spectra of Cr, NAA, Glu and Gln from simulation, a series of estimation problems are set up in order to evaluate the performance of 2DJ-PRESS and CT-PRESS on estimating individual metabolite concentrations.

In an estimation problem for spectroscopic data obtained from a scanner, individual metabolite concentrations in the scanned object are estimated with a priori information regarding the chemical shifts, phase and T1 and T2 relaxation times of each metabolite. This information is obtained either from separate reference acquisitions or from simulated spectra. The metabolite spectra simulated in SPINEVOLUTION were applied as a priori information and grouped together to form a matrix of basis functions Φ for estimation. To simulate spectroscopic data x obtained from the scanner, individual metabolite spectra were weighted in their approximate physiological concentration ratios of the brain and added to noise to form a simulated spectroscopic data. Cr, NAA, Glu and Gln were weighted in the concentration ratio 10: 12.5: 12.5: 3 and white Gaussian noise was added to the combined spectrum such that SNR of NAA = 20. Once this matrix of basis functions Φ, and the spectroscopic data vector x were formed, the estimation problem was solved by linear least-squares method for the individual metabolite concentrations $\hat{a}_1$, $\hat{a}_2$, $\hat{a}_3$ and $\hat{a}_4$.

$$\hat{a} = Re[(\Phi^*\Phi)^{-1}\Phi^* x] \tag{4.1}$$

$$Var(\hat{a}) = E[(\hat{a} - a)^2] = E[Re[(\Phi^*\Phi)^{-1}\Phi^* n]^2] \tag{4.2}$$

The accuracy of the estimation can be assessed by determining the bias and variance of the estimates. It has been shown that the estimates â are unbiased and that the variances of the estimates are of the form of Eq. 4.2 [28] where n is the noise vector added to the spectroscopic data. The variances of the estimates â depend on the orthogonality and energy of the basis functions from Cr, NAA, Glu and Gln in the matrix Φ, which we evaluate in the next section. Numerical values of the bias and variances were obtained from 3000 monte-carlo trials with different realizations of the noise with the same standard deviation.

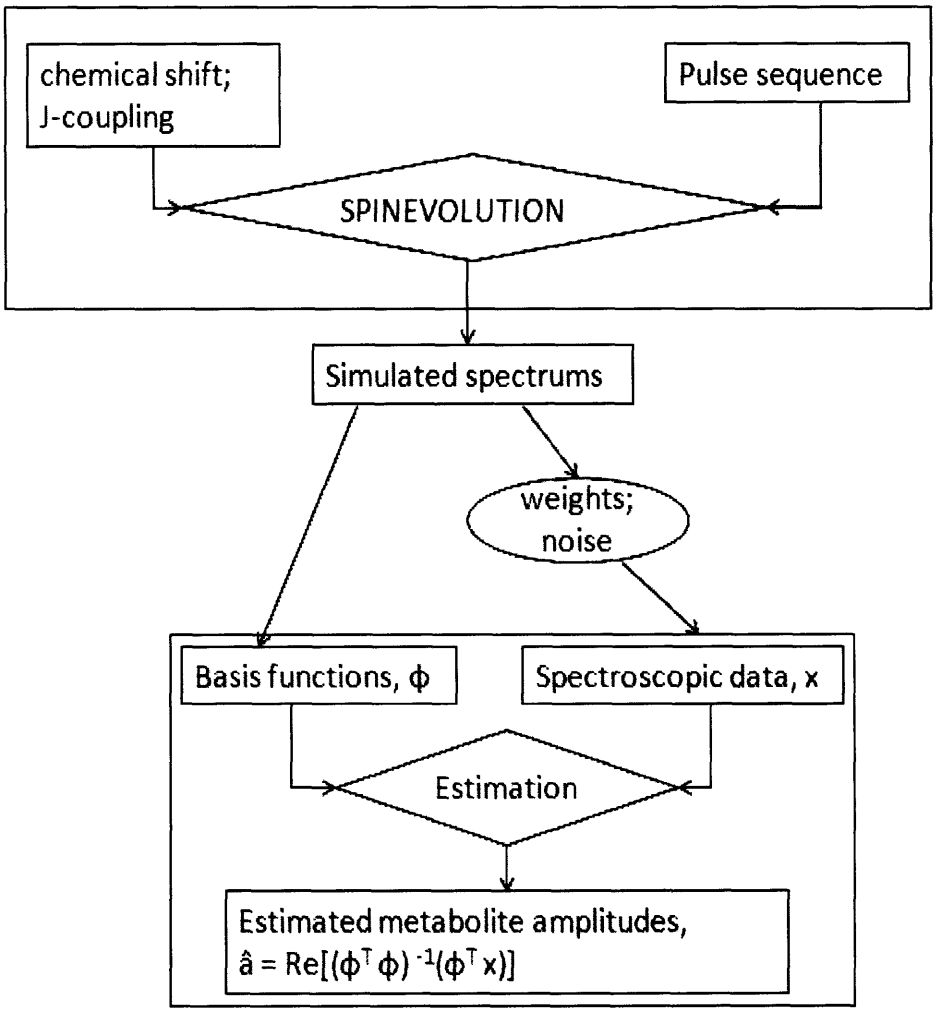

Figure 22. The set-up and solution of the estimation problem from simulated spectra. Simulated basis functions are weighted and added with noise to form the simulated spectroscopic data.

4.4. *Orthogonality of basis functions from simulated spectra*

The orthogonality between two spectra is determined by the amount of overlap between them. It is expected that the estimates â of the individual metabolite concentrations will become less accurate with greater overlap and reduced orthogonality. In this section, the differences in orthogonality of all pairings of metabolites generated from the 2DJ-PRESS, CT-PRESS and 1D spin-echo at TE=35ms sequences were analyzed. Orthogonality is defined and calculated by the inner product between the simulated spectra.

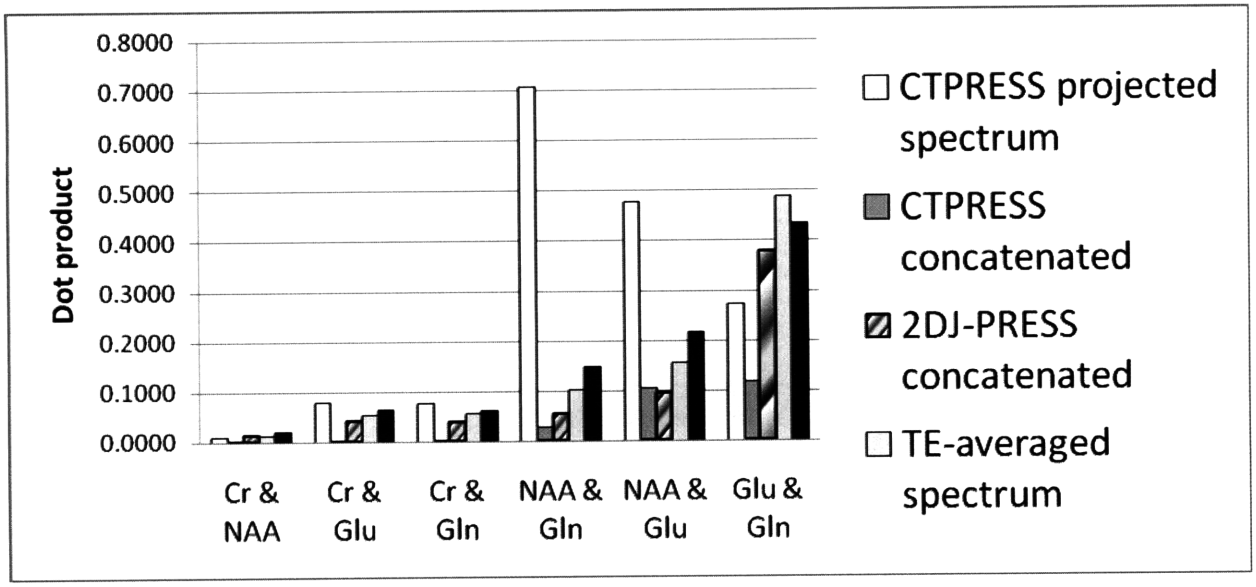

Figure 23. Inner product of noise-free 1D spectra obtained from 2D-JPRESS, CT-PRESS and 1D spin-echo at TE = 35ms simulations.

Figure 23 shows the values of the inner products evaluated between different metabolites generated from different 1D spectra obtained from the 2DJ-PRESS, CT-PRESS and 1D-spin-echo experiments, namely the TE-averaged spectrum, CT-PRESS projected spectrum and spectra of the concatenated FID's from 2D-PRESS and CT-PRESS. The orthogonality measure in Figure 23 supports known chemical shift information of the overlap between metabolite spectra. Of the 4 metabolites, Glu and Gln has the greatest spectral overlap, followed by NAA and Glu and NAA and Gln. This order of spectral overlap is reflected

in the values of the inner product s of the basis functions generated from all the schemes except for that of the projected spectrum from CT-PRESS. The projected spectrum from CT-PRESS is successful at maintaining orthogonality between Glu and Gln at a tradeoff of reduced orthogonality between NAA and Gln, and NAA and Glu.

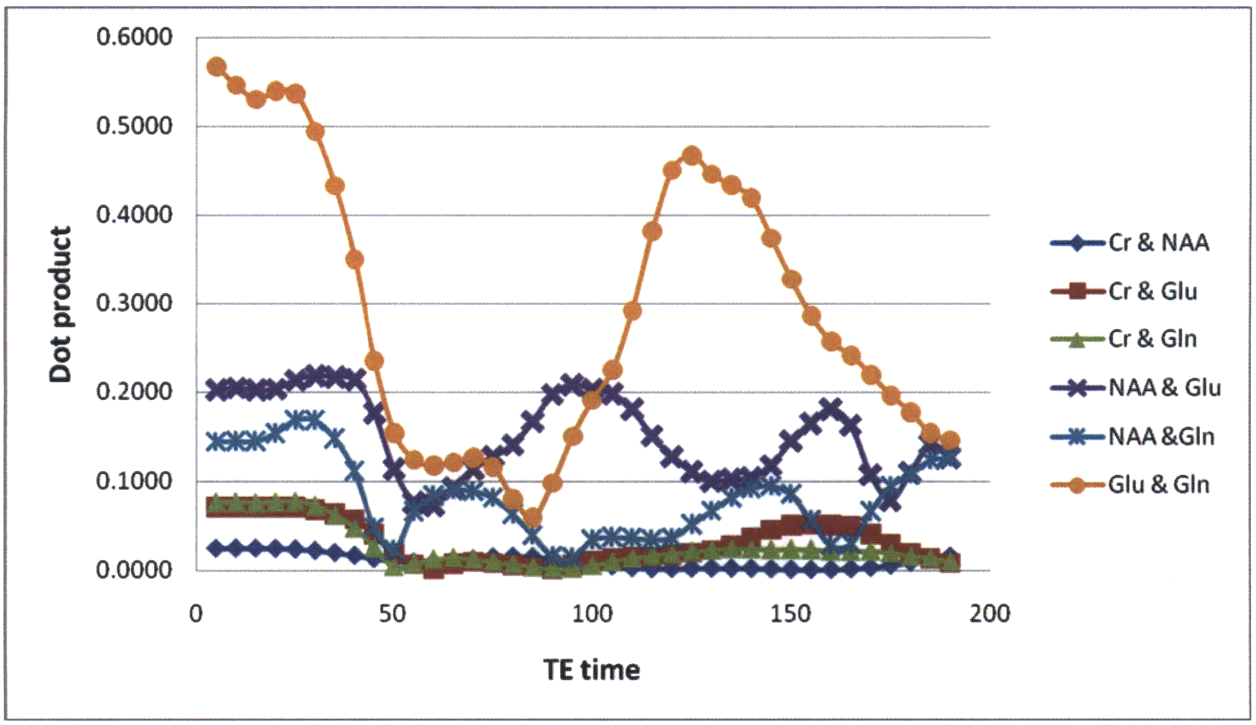

Figure 24. Inner product of noise-free metabolite basis functions for each TE step of a 38-step 2DJ-PRESS experiment.

The inner product of metabolite basis functions from each individual FID of each step of the 2DJ-PRESS and the CT-PRESS experiment was also evaluated and shown in Figure 24 and Figure 25. From Figure 24, the orthogonality of the basis functions varies as a function of TE, and this variation is especially great for the three pairings of NAA & Gln, NAA & Glu and Glu & Gln which gave the largest inner product values and least orthogonality in Figure 23. In particular, TE times between 50ms and 85ms gave the greatest orthogonality between Glu and Gln which we aim to detect independently. This TE range between 50ms and 85ms indicates an optimal subset of TE time steps necessary to obtain good signal separation of Glu and Gln.

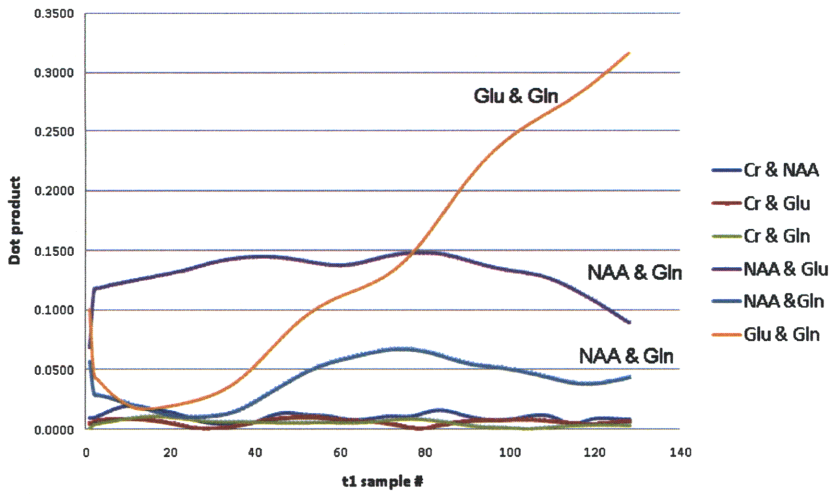

Figure 25. Inner product of noise-free metabolite basis functions for each t_1 step of a 128-step CT-PRESS experiment.

Variations in the inner product values for each t_1 step in a CT-PRESS experiment are more subtle than that for 2DJ-PRESS experiment. For increased orthogonality between Glu and Gln, the earlier t1 steps perform better in terms of inner product values. It is noted that the maximum value of the inner product between Glu and Gln is 0.32 for CT-PRESS, compared to 0.58 for 2DJ-PRESS in Figure 24.

4.5. Bias and variance in estimates â of metabolite concentrations

In this section, we evaluate the accuracy of the estimates of metabolite concentrations determined from a priori information of a matrix of basis functions and spectroscopic data built from simulated spectra appropriately weighted and combined. Plotted in Figure 26 is the average of the metabolite concentration estimates â obtained from the estimation problem applied to each t_1 step of the 2D-JPRESS and CT-PRESS simulation, averaged across 3000 trials with random realization of noise. â as calculated from Eq. (4.1) is an unbiased estimate of the metabolite concentrations and this is supported by the results shown in Figure 26. The standard deviation associated with estimating Gln high because of the low relative metabolite concentration and spectrum overlap with Glu.

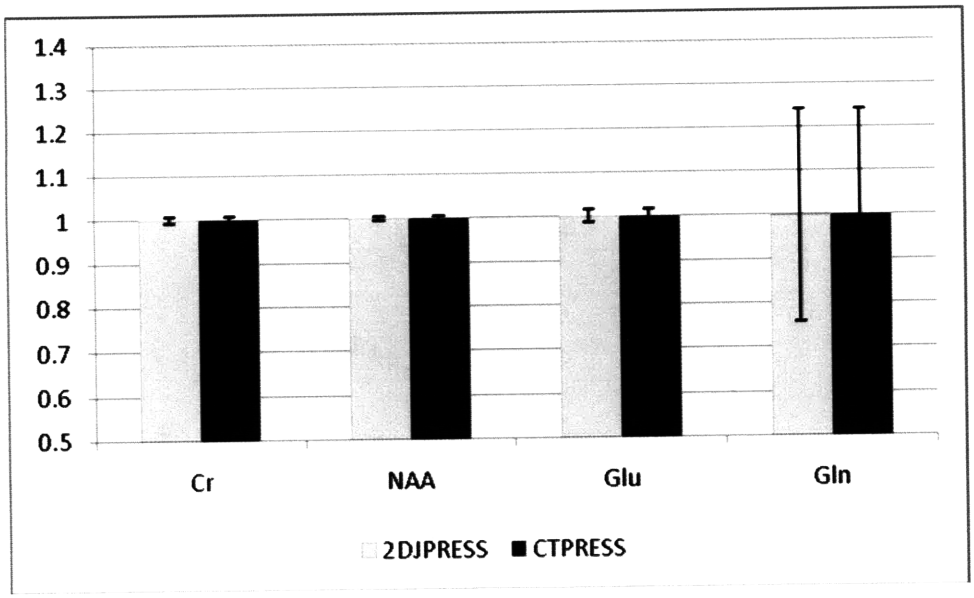

Figure 26. Average of estimates â of metabolites of interest for a 38-step 2D-JPRESS and 128-step CT-PRESS simulation shown with corresponding standard deviation bars.

The variation in standard deviation of the metabolite concentration estimates â with each individual t_1 step of the 38-step 2DJ-PRESS for the four metabolites are shown in Figure 27, Figure 28, Figure 29 and Figure 30. The standard deviations are normalized with the signal energy of the respective metabolite basis function for the first TE step. For Cr and NAA, the variation in standard deviation is due mainly to the increasing T2 decay of metabolite signal as TE increases. Glu and Gln however exhibit peaks and troughs that could be exploited in selecting a subset of TE times for better separation of Glu and Gln. It is noted that the standard deviations of concentration estimates for Cr and NAA are much lower than that for Glu and Gln, with the standard deviation for the estimation of Cr concentration being approximately 15 times lower than for Glu. The standard deviations of metabolite concentration estimates obtained from the spectrum of concatenated FID's of the 16-step 2DJ-PRESS experiment, TE-averaged PRESS and 1D spin-echo experiment at TE = 35ms are included for comparison purposes. The standard deviation of the concentration estimate for each metabolite for the 2DJ-PRESS-

concatenated spectrum represents an average of the standard deviation obtained across the individual TE's.

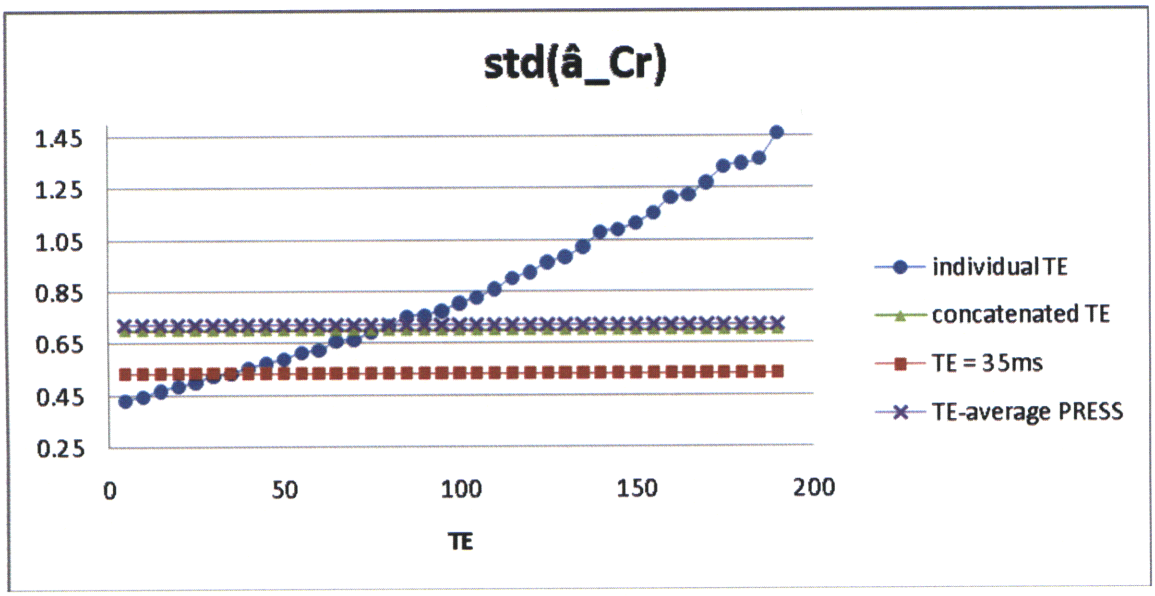

Figure 27. Standard deviation of the estimate of concentration of Cr normalized with the signal energy in the basis function of the metabolite Cr. Standard deviation shows variation with TE of a 38-step 2DJ-PRESS sequence.

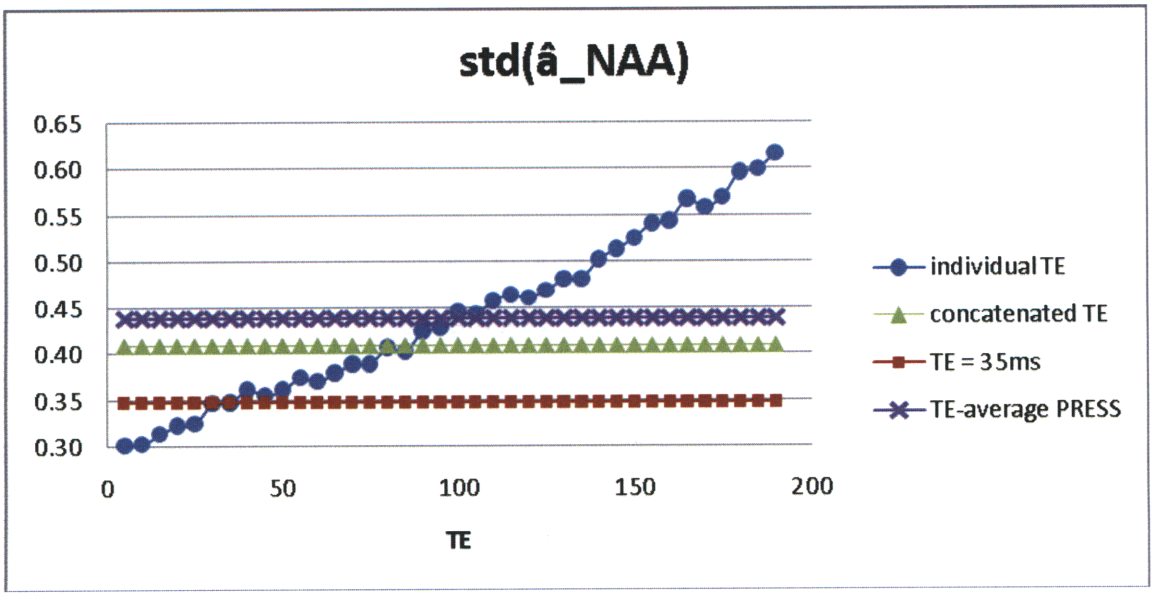

Figure 28. Standard deviation of the estimate of concentration of NAA normalized with the signal energy in the basis function of the metabolite NAA. Standard deviation shows variation with TE of a 38-step 2DJ-PRESS sequence.

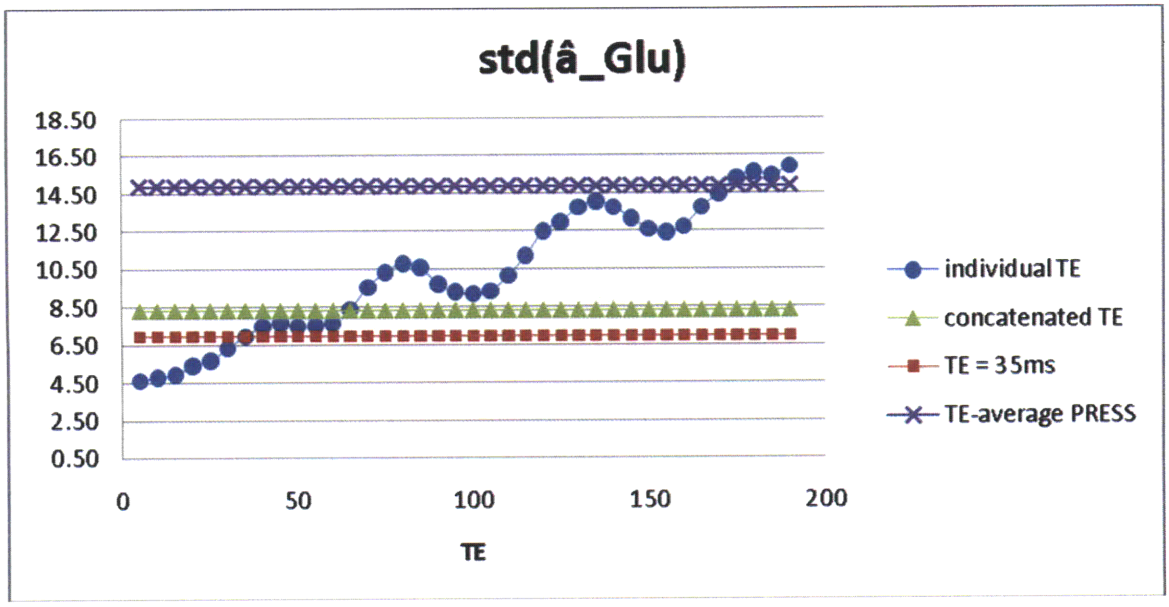

Figure 29. Standard deviation of the estimate of concentration of Glu normalized with the signal energy in the basis function of the metabolite Glu. Standard deviation shows variation with TE of a 38-step 2DJ-PRESS sequence.

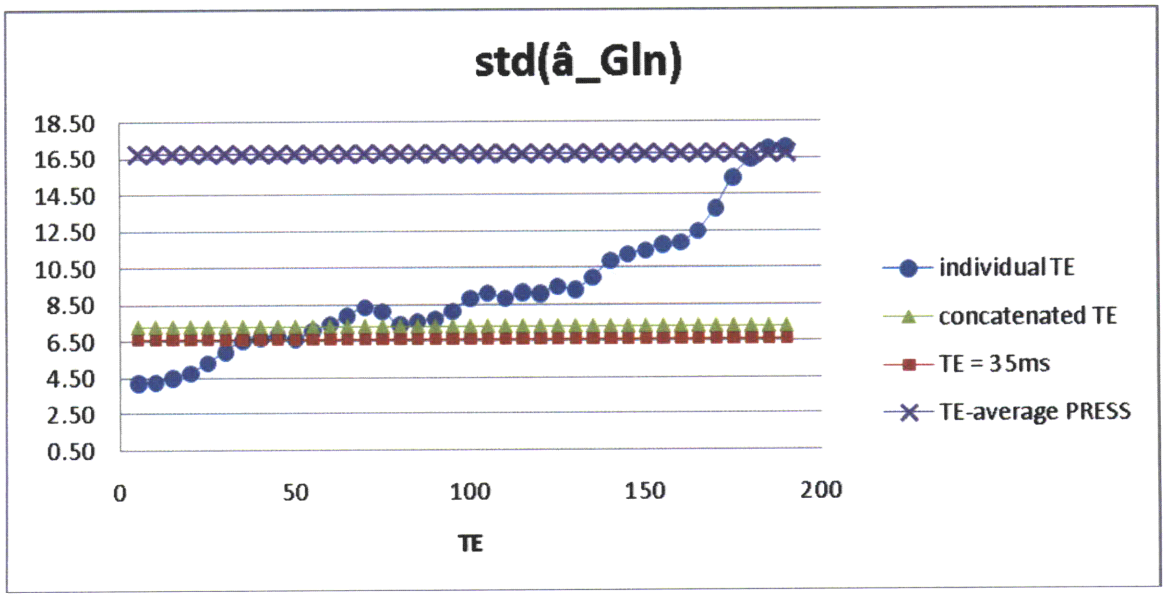

Figure 30. Standard deviation of the estimate of concentration of Gln normalized with the signal energy in the basis function of the metabolite Gln. Standard deviation shows variation with TE of a 38-step 2DJ-PRESS sequence.

Figure 31, Figure 32, Figure 33, Figure 34 and Figure 35 illustrates the variation in standard deviation of the metabolite concentration estimates â with each individual t_1 step of the CT-PRESS simulation for the four metabolites. As with the plots for 2DJ-PRESS, the standard deviations are normalized with the signal energy of the respective metabolite basis function for the first t_1 step. Due to the constant time interval during which the last 180° pulse is shifted in CT-PRESS, variations in standard deviation with t_1 are more subtle that seen for the 2DJ-PRESS experiment. A zoomed-in view shows variation in standard deviation that correlates with the variation in signal energy of the basis functions of each metabolite for individual t_1 steps. This variation in standard deviations of the metabolite concentration estimates may also be exploited for better separation of Glu and Gln but will not have as large an improvement due to the small scale of the variations. It is noted that the standard deviations of concentration estimates for Cr and NAA are much lower than that for Glu and Gln, with the standard deviation for the estimation of Cr concentration being approximately 30 times lower than for Glu.

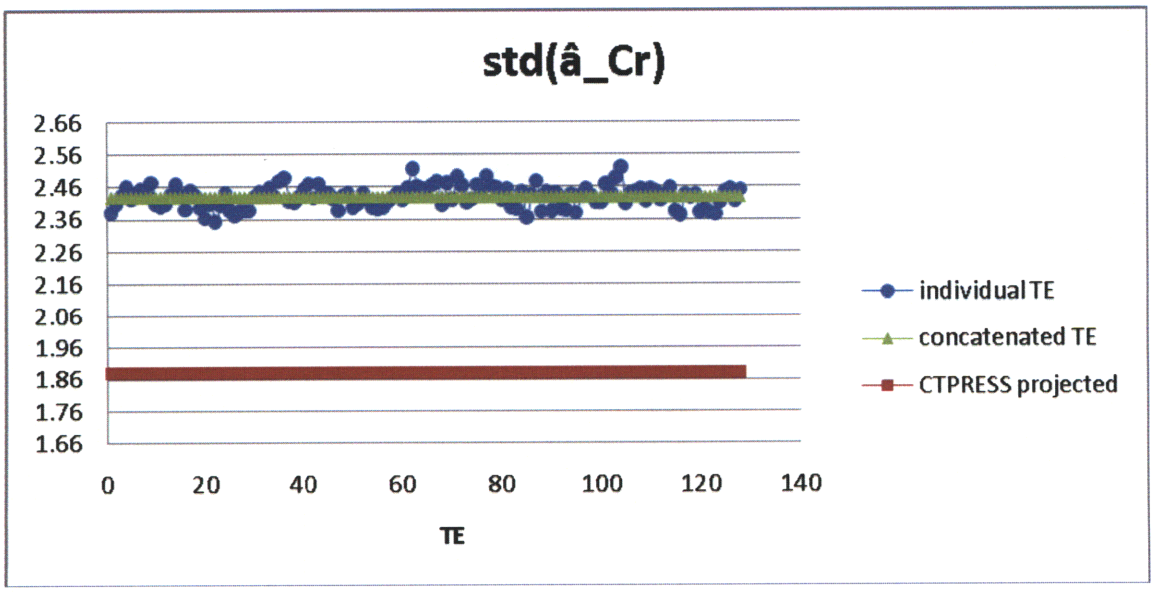

Figure 31. Standard deviation of the estimate of concentration of Cr normalized with the signal energy in the basis function of the metabolite Cr. Standard deviation shows little variation with t1 step of the CT-PRESS sequence.

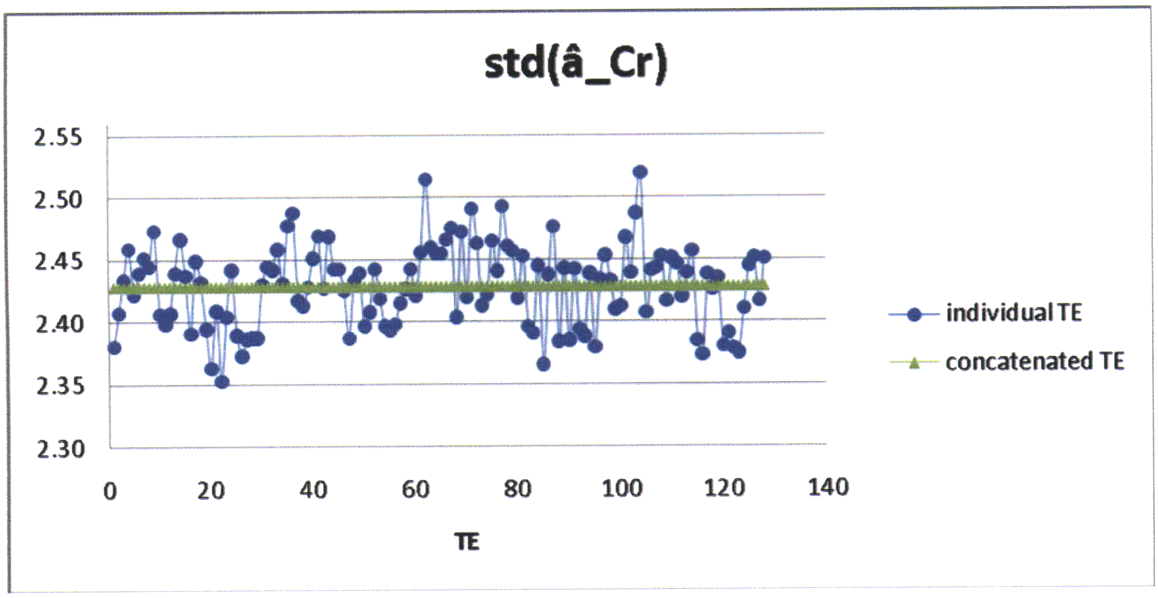

Figure 32. Zoomed view of the standard deviation of the estimate of concentration of Cr normalized with the signal energy in the basis function of the metabolite Cr. Standard deviation shows little variation with t1 step of the CT-PRESS sequence.

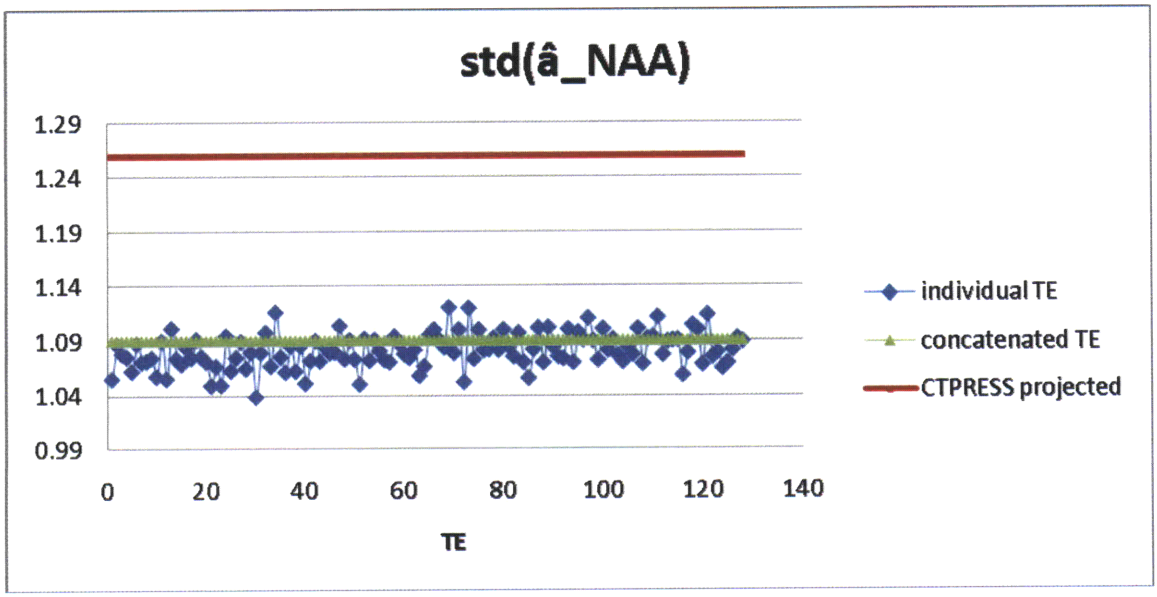

Figure 33. Standard deviation of the estimate of concentration of NAA normalized with the signal energy in the basis function of the metabolite NAA. Standard deviation shows little variation with t1 step of the CT-PRESS sequence

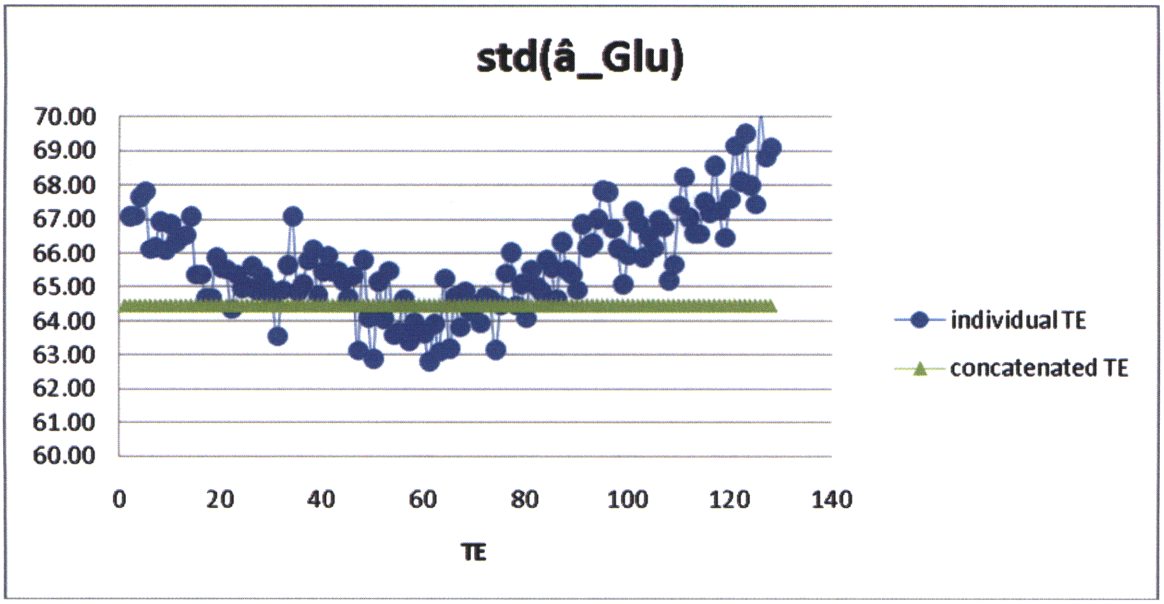

Figure 34. Zoomed view of the standard deviation of the estimate of concentration of Glu normalized with the signal energy in the basis function of the metabolite Glu. Standard deviation shows little variation with t1 step of the CT-PRESS sequence.

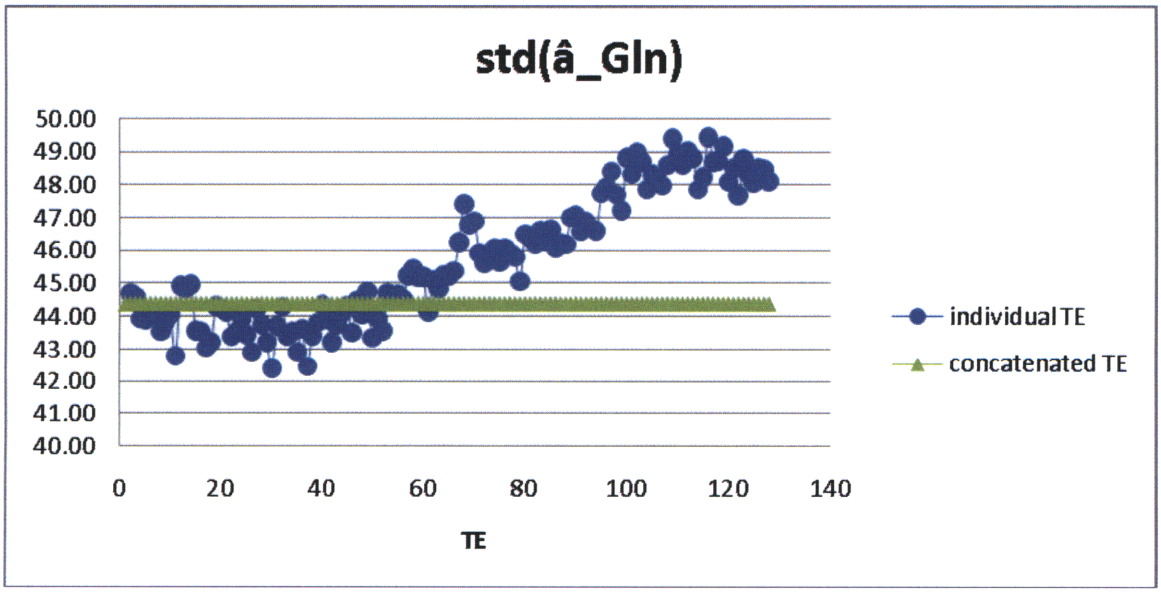

Figure 35. Zoomed view of the standard deviation of the estimate of concentration of Gln normalized with the signal energy in the basis function of the metabolite Gln. Standard deviation shows little variation with t1 step of the CT-PRESS sequence.

5. Experimental analysis of 2D-JPRESS and CT-PRESS

This chapter focuses on the analysis and processing of data acquired from 2D-JPRESS and CT-PRESS pulse sequences implemented on a 3T MRI scanner. The scans were carried out on home-made phantoms containing the same metabolites of Cr, NAA, Glu and Gln that were evaluated with simulated spectra. This work is in preparation for the estimation of metabolites concentrations in vivo or in a phantom containing a mix of metabolites, where the FID and spectra acquired for each metabolite is taken to be the basis function for that metabolite in the estimation problem.

5.1. Method

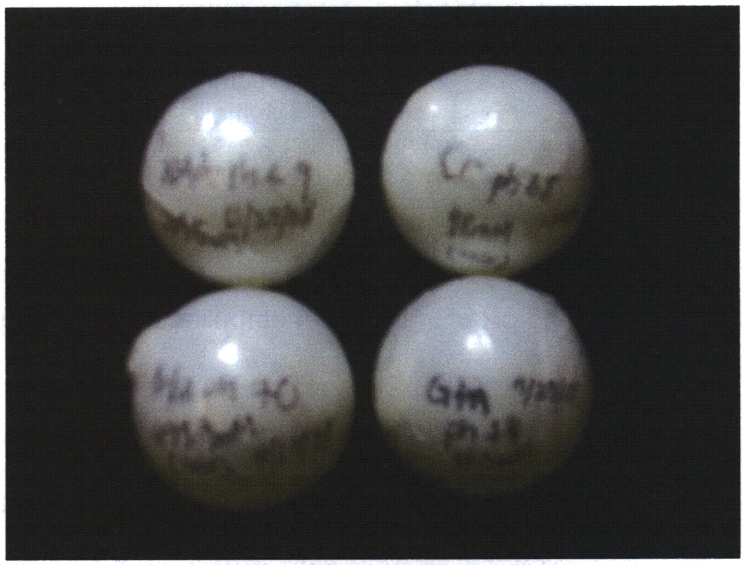

Figure 36. Concentrated solutions of Cr, NAA, Glu and Gln at 98mM, 251mM, 500mM and 180mM respectively were injected into different ping-pong balls of diameter 40mm. The opening was sealed with wax before wrapping the phantom with Parafilm

Solutions of Cr, NAA, Glu and Gln were made by dissolving the powder form of creatine monohydrate, N-Acetyl-L-aspartic acid, L-Glutamic acid (Sigma-Aldrich, Missouri, USA) and L-Glutamine (Hyclone Laboratories Inc., Utah USA) respectively in water to create concentrated

metabolite solutions. The pH of each solution was adjusted to around 7.0 with sodium hydroxide and potassium phosphate monobasic (Sigma-Aldrich, Missouri, USA). 0.1% of sodium azide (Sigma-Aldrich, Missouri, USA) was also added to each metabolite solution. The concentrations and pH of each solution are summarized in Table 1. The concentrations of the solutions of Cr, NAA, Glu and Gln are multiple times than they would be in a regular spectroscopy phantom for increased SNR [29]. Phantoms were made by injecting the metabolite solutions into individual ping-pong balls (diameter 40mm) and sealing the opening with wax. Several layers of Parafilm were wrapped around each ping-pong ball to reduce evaporation from micropores. The phantoms are shown in Figure 36. Due to Gln being unstable in solution **Error! Reference source not found.**, the spectroscopy scan was done within 6 hours of the making of the phantoms.

Metabolite	Concentration (mM)	pH	Concentration relative to standard spectroscopy phantom [29]. (Multiplicative factor)
Cr	98	6.8	9.8
NAA	251	6.9	20.1
Glu	500	7.0	40.0
Gln	180	7.4	60.0

Table 2. Concentrations and pH of individual metabolite solutions injected into phantoms

All imaging was done on a 3.0 T MRI scanner (Siemens AG, Erlangen, Germany) and with a 32-channel head-coil for increased SNR. A spectroscopic voxel of size 20mm x 20mm x 20mm was placed in the center of the ping-pong ball, away from the air bubble at the opening where the solutions were injected. The voxel for the 2D-JPRESS MRS was excited using CHESS water suppression at 16 TE steps ranging from 35ms to 185 ms and TR = 2s. 4 preparation scans and 20 averages for each TE step resulted in a total scan-time of 10:48min. The voxel for CT-PRESS MRS was excited with CHESS water suppression and PRESS at TE = 35ms and TR =2s. 4 preparation scans and 20 averages for each TE step resulted in a total

scan-time of 21:28min. The spectra bandwidth was at 1000 Hz with 1024 ADC points and the water suppression bandwidth was at 35 Hz for both pulse sequences. The application of the last 180° pulse was varied in 32 t_1 steps in increments of 4ms shown in Figure 37. This violates Nyquist sampling but metabolites spectrum are successfully recovered because the signal in a 2D CT-PRESS spectrum is only along the diagonal [14]. The CT-PRESS projected spectrum was obtained by unwrapping the 2D spectrum along f_1 and integrating the spectra along f_2 within a ±13Hz interval around the diagonal spectra. The CT-PRESS concatenated spectrum was obtained from the concatenation of the 32 FID's from each of the t_1 step.

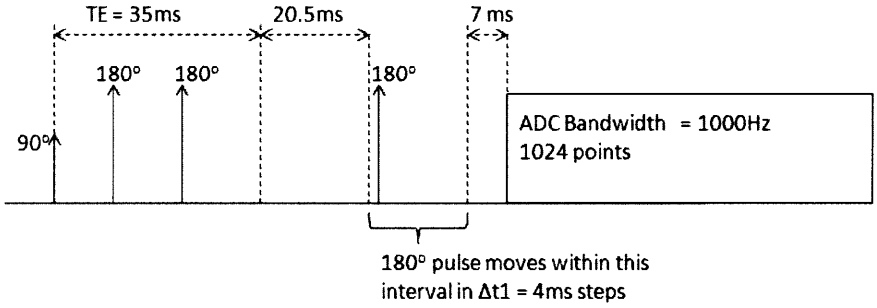

Figure 37. Timing parameters for the CT-PRESS experiment implemented on scanner. PRESS was implemented with TE = 35ms. The location of the last 180o pulse is varied in 32 steps resulting in undersampling in t1.

5.2. Orthogonality of basis functions from scan

Basis functions for each metabolite were formed from the spectra of the 2D-JPRESS and CT-PRESS acquisition for each ping-pong ball phantom. The orthogonality between two spectra of each pairing of metabolites is evaluated and shown in Figure 38. Orthogonality is defined and calculated by the inner product between the spectra of various pairings of different metabolites. As shown in Figure 38, the orthogonality measure supports known chemical shift information of the overlap between metabolite spectra, where the orthogonality between Glu and Gln is the least, followed by the orthogonality between NAA and Glu, and NAA and Gln. It is

noted that the projected spectrum from CT-PRESS and the TE-averaged spectrum provides the greatest orthogonality of the Glu and Gln spectra while the 1D spin echo at TE = 35 provides the least orthogonality.

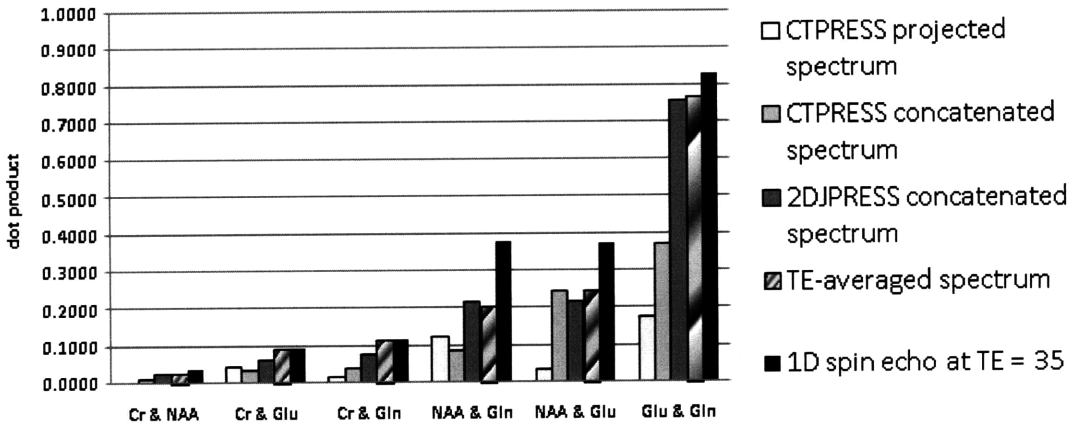

Figure 38. Inner product of spectra obtained from 2D-JPRESS, CT-PRESS and 1D spin-echo at TE = 35ms acquisitions at 3.0T scanner

The inner products of metabolite spectra from each FID of individual t_1 steps of the 2D-JPRESS and the CT-PRESS experiments were also evaluated and shown in Figure 39 and Figure 40. For both 2D-JPRESS and CT-PRESS, the orthogonality of the basis functions varies as a function of t, and this variation is especially great for the three pairings of NAA & Gln, NAA & Glu and Glu & Gln which also gave the greatest inner product values and least orthogonality in Figure 38. In particular, TE times between 55ms and 75ms of the 2D-PRESS experiment gave the greatest orthogonality values for the pairing of Glu and Gln. The TE range between 55ms and 100ms indicates an optimal subset of TE time steps necessary for good signal separation of Glu and Gln. Variations in the inner product values with the 32 t_1 step in a CT-PRESS experiment are of the same scale as that for the 2DJ-PRESS experiment. t_1 value between the 9^{th} and 14^{th} step of the CT-PRESS experiment produced Glu and Gln spectra with increased orthogonality.

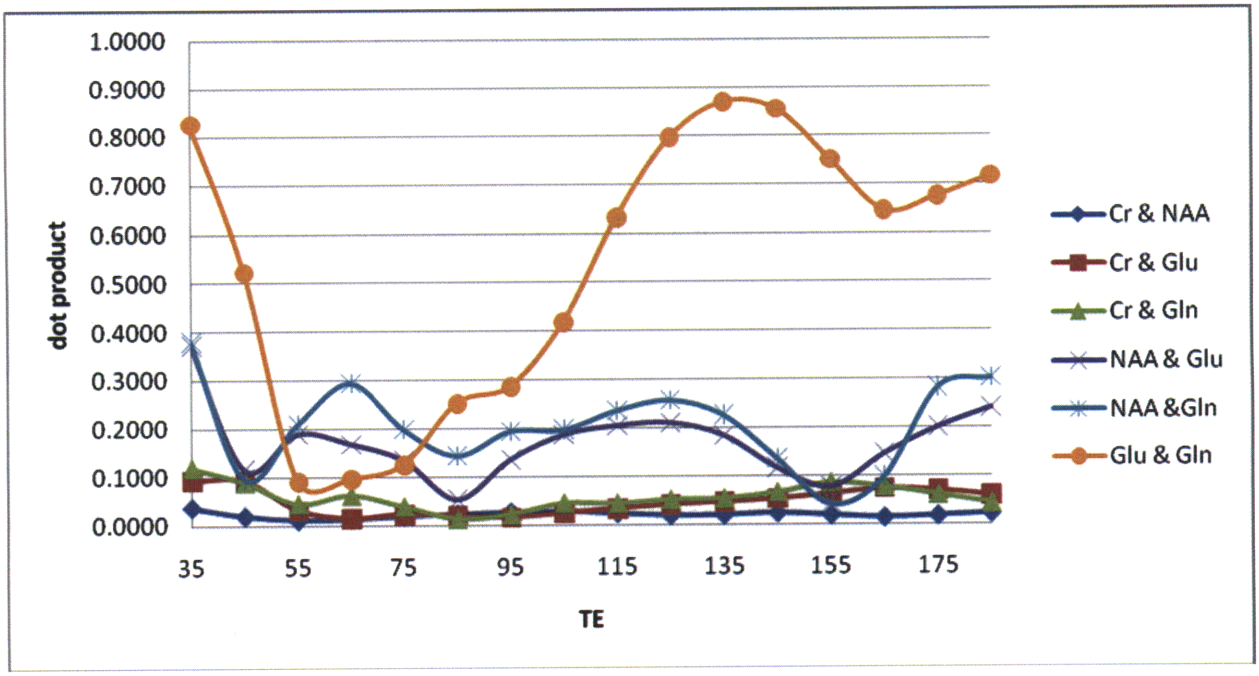

Figure 39. Inner product of metabolite basis functions for each TE step of a 16-step 2DJ-PRESS experiment implemented on a 3.0 T scanner

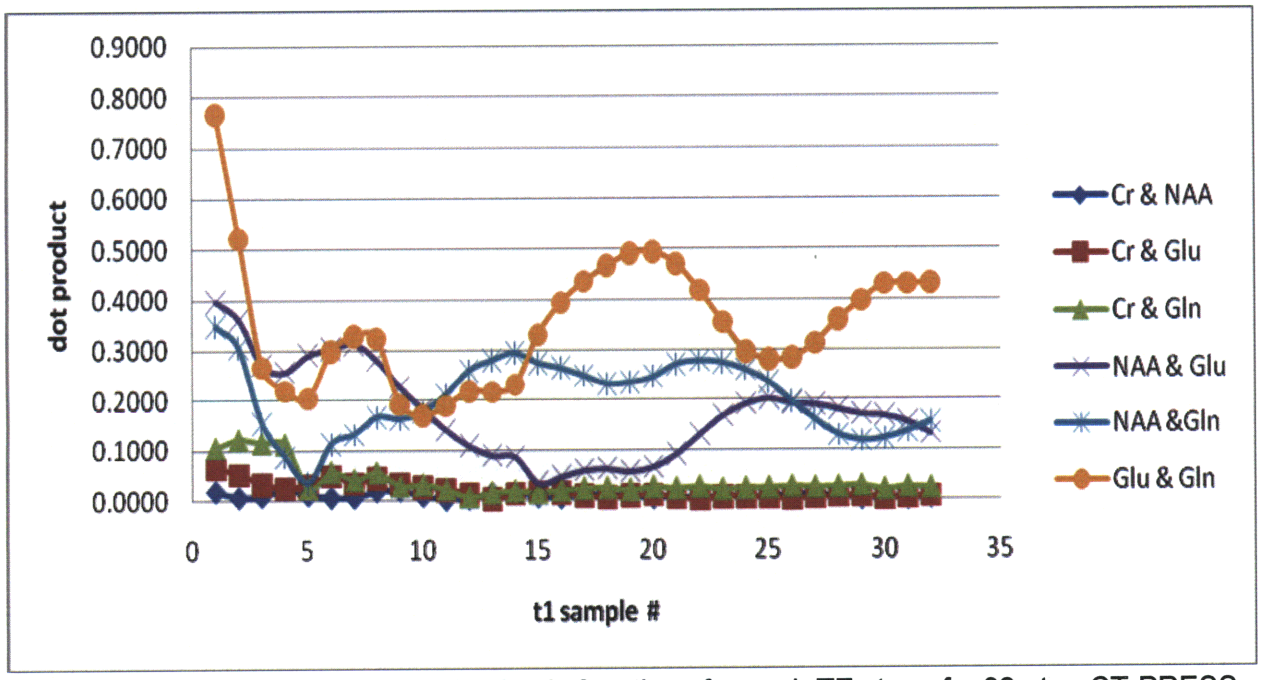

Figure 40. Inner product of metabolite basis functions for each TE step of a 32-step CT-PRESS experiment implemented on a 3.0 T scanner

6. Experimental analysis of 2D-JPRESS and CT-PRESS

MRS involves the detection and mapping of much weaker signals from brain metabolites. Limited chemical shift dispersion and J-coupling causes spectral overlap and complicated spectral shapes that limit detection and separation of several brain metabolites. The first part of this thesis combines 1D spectroscopy with segmented structural data in the compartmental analysis of ratio measures of metabolite concentrations.

The second part of this thesis studied the effectiveness of 2D-JPRESS and CT-PRESS, which employ additional encoding steps in a second time axis t_1 at estimation of metabolite concentrations. The additional encoding steps result in a penalty of increased scan time and this work attempted to evaluate and analyze the effects of different t_1 times on the orthogonality between metabolite spectra and variances in the estimates of metabolite concentrations, both through simulations and experiments on a 3T MRI scanner.

6.1. Discussion

There is an observable variation in orthogonality and standard deviation in the metabolite concentration estimates from the simulation and experiments done on the 3T MRI scanner for a 2DJ-PRESS sequence. Focusing on the orthogonality of Glu and Gln spectra, simulation data of the 2DJ-PRESS sequence shows that the greatest orthogonality occurs around 55ms – 85ms. The simulation results approximate the range of 55ms – 75ms indicated from experiments done on the scanner. Simulation of the 128-step CT-PRESS sequence shows that the variation in orthogonality and standard deviation in metabolite estimates are more subtle and would improve at earlier t_1 steps. To reduce the scan-time for the CT-PRESS experiment done on the 3T MRI scanner, an under-sampled 32-step CT-PRESS sequence was implemented and used. The variation with t_1 of the orthogonality of Glu and Gln spectra for the 32-step CT-PRESS sequence

is more substantial than that for the 128-step CT-PRESS sequence. It is noted that the orthogonality between the Glu and Gln spectra were the greatest in the range of $16ms<t_1<20ms$ between the 9^{th} and 11^{th} step. The range of t_1 steps for the 2D-JPRESS and CT-PRESS represents a possible subset of optimal t_1 times for which the total scan-time can be shortened while maintaining quality of separation of Glu and Gln.

In addition to evaluating orthogonality and standard deviation at each t_1 step for CT-PRESS and 2D-JPRESS, the 1D spectra that result from averaging across TE's from the 2D-JPRESS spectra (TE-averaged spectrum), projecting the 2D CT-PRESS spectrum onto the f1 axis (CT-PRESS projected spectrum), concatenating all available FID's from each t1 step (2D-JPRESS concatenated and CT-PRESS concatenated spectra), and the 1D spin echo at TE = 35ms were also studied. Results from experiments done on the scanner shows that the CT-PRESS projected and TE-averaged spectra performed the best in terms of orthogonality between Glu and Gln spectra. These findings were not predicted by the same orthogonality evaluation done on the simulated 2D-JPRESS and CT-PRESS sequences. This may be due to a greater robustness of the CT-PRESS projected and TE-averaged technique to non-ideal conditions than the 1D spin-echo and concatenated spectra. While the simulated spectra of the basis functions from the 2D-JPRESS and CT-PRESS sequences are ideal and noise-free, the spectra obtained from the scanner include noise contributions as well as magnetic field inhomogeneities.

6.2. Future work

A potential subset of optimal t_1 times has been identified for both the 2DJ-PRESS and CT-PRESS sequences. This subset of t_1 times will be tested in the estimation of metabolite concentrations in phantoms containing a mix of metabolites similar to physiological

concentration ratios. Reduced sampling of this subset of range of t_1 time for application at higher field strengths will be explored in further analysis.

7. Appendix

7.1. Simulation input files for SPINEVOLUTION

Examples of the simulation input files for Glu of the 1D-spin-echo, 2DJ-PRESS and CT-PRESS experiments are presented in this section. In all of the examples below, lines containing only asterisk represent the default setting and are omitted. To avoid repetition, the T1 and T2 relaxation parameters of only the first numbered proton of Glu at chemical shift 3.7433ppm are shown, and the T1 and T2 parameters of the rest of the protons are represented by (.... ....).

7.1.1. 1D spin- echo experiment at TE=35ms

This example is of a 1D spin-echo experiment at TE = 35 ms for Glu at 3T B_0 field strength with very short rectangular 90° and 180° pulses. Acquisition is at 5000Hz bandwidth and 2000 ADC points are collected. T1 and T2 relaxation is implemented throughout the sequence.

```
****** The System ***********************
spectrometer(MHz)    128
channels             H1
nuclei               H1 H1 H1 H1 H1
cs_isotropic         3.7433 2.0375 2.1200 2.3378 2.3520 ppm
j_coupling           1 2 7.331
j_coupling           1 3 4.651
j_coupling           2 3 -14.849
j_coupling           2 5 8.406
j_coupling           3 5 6.875
j_coupling           2 4 6.413
j_coupling           3 4 8.478
j_coupling           4 5 -15.915
******* Pulse Sequence ******************************
CHN 1
timing(usec)         0.5   17500  0.5   17500  (200)2000D1
power(kHz)           500   0      1000  0       0
phase(deg)           0     0      90    0       0
freq_offs(kHz)       0     0      0     0       0
******* Variables ***********************************
ppm_ref_offs_1 = 0
variable T1SQ_1_1 = 1230
variable T2SQ_1_1 = 200
variable T1SQ_1_2 = 1230
```

```
variable T2SQ_1_2 = 200
(............)
******* Options ************************************
rho0                Flz
observables         Flp
line_broaden(Hz)    0 0
FFT_dimensions
```

7.1.2. 16-step 2DJ-PRESS experiment

This example is of a 2D-JPRESS experiment as shown in Figure 20 for Glu at 3T B_0 field strength with TE ranging from 35ms to 185ms in increments of 10ms. The sequence is simulated with very short rectangular 90° and 180° pulses, and T1 and T2 relaxation is implemented throughout the sequence. Acquisition is at 5000Hz bandwidth and 2000 ADC points are collected.

```
****** The System ***********************
spectrometer(MHz)   128
channels            H1
nuclei              H1 H1 H1 H1 H1
cs_isotropic        3.7433 2.0375 2.1200 2.3378 2.3520 ppm
j_coupling          1 2 7.331
j_coupling          1 3 4.651
j_coupling          2 3 -14.849
j_coupling          2 5 8.406
j_coupling          3 5 6.875
j_coupling          2 4 6.413
j_coupling          3 4 8.478
j_coupling          4 5 -15.915
******* Pulse Sequence *****************************
CHN 1
timing(usec)    0.5  8750 (2500)16D1 0.5  17500 (5000)16D1 0.5  8750 (2500)16D1 (200)2000D2
power(kHz)      500 0     0          1000 0     0          1000 0    0          0
phase(deg)      0   0     0          0    0     0          0    0    0          0
freq_offs(kHz)  0   0     0          0    0     0          0    0    0          0
******* Variables **********************************
ppm_ref_offs_1 = 0
variable T1SQ_1_1 = 1230
variable T2SQ_1_1 = 200
variable T1SQ_1_2 = 1230
variable T2SQ_1_2 = 200
variable T1SQ_1_3 = 1230
variable T2SQ_1_3 = 200
variable T1SQ_1_4 = 1230
variable T2SQ_1_4 = 200
variable T1SQ_1_5 = 1230
variable T2SQ_1_5 = 200
variable T1SQ_1_6 = 1230
```

```
variable T2SQ_1_6 = 200
variable T1SQ_1_7 = 1230
variable T2SQ_1_7 = 200
(............)
******* Options ************************************
rho0                F1z
observables         F1p
line_broaden(Hz)    0 0 0 0
FFT_dimensions
```

7.1.3. 128-step CT-PRESS experiment

This example is of a CT-PRESS experiment as shown in Figure 19 for Glu at 3T B_o field strength with t_1 ranging in increments of 133us. The sequence is simulated with very short rectangular 90° and 180° pulses, and T1 and T2 relaxation is implemented throughout the sequence. Acquisition is at 5000Hz bandwidth and 2000 ADC points are collected.

```
****** The System **********************
spectrometer(MHz)   128
channels            H1
nuclei              H1 H1 H1 H1 H1
cs_isotropic        3.7433 2.0375 2.1200 2.3378 2.3520 ppm
j_coupling          1 2 7.331
j_coupling          1 3 4.651
j_coupling          2 3 -14.849
j_coupling          2 5 8.406
j_coupling          3 5 6.875
j_coupling          2 4 6.413
j_coupling          3 4 8.478
j_coupling          4 5 -15.915
******* Pulse Sequence *****************************
CHN 1
timing(usec)    0.5  3500 0.5  7000 0.5  3500 31000 8500 (133)128D1  0.5  (133)-128D1 8500
(266)2000D2
power(kHz)      500  0   1000  0   1000  0   0    0   0      1000  0      0   0
phase(deg)      0   0   0   0   0   0   0   0   0      0   0      0   0
freq_offs(kHz)  0   0   0   0   0   0   0   0   0      0   0      0   0
******* Variables **********************************
ppm_ref_offs_1 = 0
variable T1SQ_1_1 = 1230
variable T2SQ_1_1 = 200
variable T1SQ_1_2 = 1230
variable T2SQ_1_2 = 200
variable T1SQ_1_4 = 1230
variable T2SQ_1_4 = 200
variable T1SQ_1_5 = 1230
variable T2SQ_1_5 = 200
variable T1SQ_1_6 = 1230
variable T2SQ_1_6 = 200
(............)
```

```
******* Options ************************************
rho0                F1z
observables         F1p
line_broaden(Hz)    0 0 0 0
FFT_dimensions
```

8. Bibliography

[1] Bloch F, "Nuclear Induction". *Physics Review*, 1946; 70:460-473.

[2] Purcell EM, Rottery HC, and Pound RV, "Resonance absorption by nuclear magnetic moments in a solid". *Physics Review*, 1946; 69: 37-38.

[3] Nishimura DG, *Principles of Magnetic Resonance Imaging.* 1996

[4] Hornak JP, *The Basics of NMR*, 1997, Retrieved from http://www.cis.rit.edu/htbooks/nmr/

[5] Vlaardingerbroek MT, den Boer JA, *Magnetic Resonance Imaging.* 1995

[6] Kok T, Ratai E-M, Eichler F, Adalsteinsson E, "Analysis of 1H Metabolite Ratios Using Image Segmentation at 7T in adult patients with X-linked Adrenoleukodystrophy", Toronto, Canada, *ISMRM Proc.*, #1596

[7] Ratai E, Kok T, Wiggins C, Wiggins G, Grant E, Gagoski B, O'Neill G, Adalsteinsson E, Eichler F, "Seven-Tesla proton magnetic resonance spectroscopic imaging in adult X-linked adrenoleukodystrophy." *Archives of neurology* 2008;65(11):1488-94

[8] Hore, PJ, Jones JA and Wimperis SA, NMR: The Toolkit, p. 28-37, 2006

[9] Govindaraju V, Young K and Maudsley AA, "Proton NMR chemical shifts and coupling constants for brain metabolites", *NMR Biomed.* 2000;13:129–153

[10] Ross BD. "Biochemical considerations in 1H spectroscopy.Glutamate and glutamine; *myo*-inositol and related metabolites." *NMR Biomed.* 1991; 4: 59–63

[11] Kreis R, Farrow N, Ross BD. "Localized 1H NMR spectroscopy in patients with chronic hepatic encephalopathy. Analysis of changes in cerebral glutamine, choline and inositols". *NMR Biomed.* 1991; 4: 109–116.

[12] Dreher W, Leibfritz D, "On the Use of Two-Dimensional-J NMR Measurements for in Vivo Proton MRS: Measurement of Homonuclear Decupled Spectra without the Need for Short Echo Times", *Magn Reson Med.* 1995; 34:331-337.

[13] Dreher W, Leibfritz D, "Detection of Homononuclear Decoupled in Vivo Proton NMR Spectra Using Constant Time Chemical Shift Encoding: CT-PRESS", *Magn. Reson. Imaging.* 1999; 17(1):141-150.

[14] Mayer D, Spielman DM, "Detection of glutamate in the human brain at 3 T using optimized constant time point resolved spectroscopy." *Magn Reson Med.* 2005; 54:439–442

[15] Hurd R, Sailasuta N, Srinivasan R, Vigneron DB, Pelletier D, Nelson SJ, "Measurement of Brain Glutamate Using TE-Averaged PRESS at 3T", *Magn Reson Med.* 2004; 51:435-440.

[16] Rothman DL, Hanstock CC, Petroff OAC, Novotny EJ, Prichard JW, Shulman RG, "Localized ^{1}H NMR Spectra of Glutamate in the Human Brain", *Magn Reson Med.* 1992; 25:94-106

[17] Provencher SW, "Estimation of Metabolite Concentrations from Localized in Vivo Proton NMR Spectra" *Magn Reson Med.* 1993; 30:672-679.

[18] Hetherinton HP, Pan JW, Mason GF, Adams D, Vaughn MJ, Twieg DB, Pohost GM, "Quantitative 1H Spectroscopic Imaging of Human Brain at 4.1T Using Image Segmentation", *Magn Reson Med.* 1996; 36:21-29

[19] Pfefferbaum A, Sullivan E, Adalsteinsson A, Spielman D, Lim KO. "In vivo spectroscopic quantification of the N-acetyl moiety, creatine and choline from large volumes of gray and white matter: effects of normal aging.", *J Magn Reson Imaging.* 1998;41:276-284

[20] Golub G, Pereyra A. "The differentiation of pseudo-inverses and nonlinear least squares problems whose variables separate." *SIAM J Num Anal* 1973;10:413–431.

[21] Fischl B, Salat DH, van der Kouwe AJW, Makris N, Ségonne F, Dale AM. "Sequence-independent Segmentation of Magnetic Resonance Images". *NeuroImage,* 2004; 23 Suppl 1, S69-84.

[22] Fischl B, Salat D, Busa E, Albert M, Dieterich M, Haselgrove C, van der Kouwe A, Killiany R, Kennedy D, Klaveness S, Montillo A, Makris N, Rosen B, Dale A.M. "Whole brain segmentation. Automated labeling of neuroanatomical structures in the human brain". *Neuron.* 2002; 33(3):341-355.

[23] Ratai E, Wiggins C, Wiggins G, Grant E, Gagoski B, Adalsteinsson E, Eichler F, "Highfield Proton MRSI in Adult Patients with X-Linked Adrenoleukodystrophy." Berlin, Germany, *ISMRM Proc.*, #769

[24] Veshtort M, Griffin RG, "SPINEVOLUTION: A Powerful Tool for the Simulation of Solid and Liquid State NMR Experiments", *J Mag Reson*, 2006; 178:248-282

[25] Traber F, Block W, Lamerichs R, Gieseke J, Schild HH. "^{1}H metabolite relaxation times at 3.0 tesla: measurements of T1 and T2 values in normal brain and determination of regional differences in transverse relaxation". *J Magn Reson Imaging* 2004;19:537–545.

[26] Srinivasan R, Sailasuta N, Hurd R, Nelson S, Pelletier D."Evidence of elevated glutamate in multiple sclerosis using magnetic resonance spectroscopy at 3 T". B*rain* 2005;128:1016-1025.

[27] Choi C, Coupland NJ, Bhardwaj PP, Kalra S, Casault CA, Reid K, Allen PS. "T2 measurement and quantification of glutamate in human brain in vivo". *Magn Reson Med* 2006;56:971–977.

[28] Spielman DM, "Magnetic Resonance Metabolic Imaging", (PhD dissertation, Stanford University, 1990) p. 52-60

[29] Schirmer T, Auer DP, "On the reliability of quantitative clinical magnetic resonance spectroscopy of the human brain", *NMR Biomed.* 2000:13:28-36

[30] L-Glutamine Stability Study1997, Retrieved from http://*www.sigmaaldrich.com/sigma/product%20information%20sheet/g3126pis.pdf*